Copyright

By

Paul Bowles

2016

Relative Timing of Structure Growth since the Deposition of the Amnicola Clay, Elk Hills, California

By

Paul Bowles

Submitted to the Department of Geological Sciences, California State University

Bakersfield

In partial fulfillment of the requirements of the degree of Masters of Geology

Spring 2016

Relative Timing of Structure Growth since the Deposition of the Amnicola Clay, Elk Hills, California

By Paul Bowles

This thesis has been accepted on behalf of the Department of Geological Science by the members of the supervisory committee:

Dr. Janice Gillespie
Committee Chair

Dr. Robert Negrini
Committee Member

Kenneth Frost, Sentinel Peak Resources
Committee Member

Table of Contents

List of Figures…….. …6

Abstract……...…..8

Introduction…….. …9

Regional Geology……...11

Statement of Problem…….....21

Methods…… ..23

Results…….…27

Discussion/Conclusion…… ...36

References…….…..40

Appendix…….…44

List of Figures

Figure 1: Regional San Joaquin Basin Map…….....…...10

Figure 2: Elk Hills Oil Field Location Map……. …12

Figure 3: Generalized Southern San Joaquin Cross Section through Study Area…….....13

Figure 4: Stratigraphic Column of the Elk Hills Region…….…… ….15

Figure 5: Paleogeography during the Deposition of the Tulare……. …..16

Figure 6: Photograph of Amnicola longinqua…….……..... ….18

Figure 7: Seismic Flooding Horizons…….……. ……19

Figure 8A: Seismic Line Location Map……..…… …….20

Figure 8B: Seismic Line with Flooding Event Horizons…….. ……...20

Figure 9: Control Points used for Log Correlation……... ..……..24

Figure 10: Amnicola Clay Type Log…….…… ……25

Figure 11: Amnicola Clay Structure Map…….. …..……..28

Figure 12: Amnicola Clay D-D' North to South Cross Section..……..... …….29

Figure 13: Amnicola Clay Isochore Map with Structural Contours…….…… ……..30

Figure 14: Tulare Clay Type Log…….…….....…… ……..32

Figure 15A: Tulare Clay F-F' West to East Cross Section…..... ……..33

Figure 15B: Tulare Clay E-E' North to South Cross Section…….…… ……..33

Figure 16: Tulare Clay Structure Map……..…….....…… ……...34

Figure 17. Tulare Clay Isochore Map…….....…… ……..…35

Appendix

1. Amnicola Clay Well Marker Spreadsheet……..…… …44
2. Tulare Clay Well Marker Spreadsheet…….……...……65
3. West to East Cross Section A-A' …….…….68
4. Northeast to Southwest Cross Section B-B'…….…….69
5. Northeast to Southwest Cross Section C-C'…….……..70
6. Northeast to Southwest Cross Section D-D''……. ……....71
7. North to South Cross Section E-E'…….…….. ……..72
8. West to East Cross Section F-F'……... …….73

Abstract

The lacustrine Amnicola Clay separates the upper and lower members of the Pleistocene-aged Tulare Formation at the Elk Hills oilfield in the southern San Joaquin Valley, California. The Tulare Clay is found within the upper Tulare Formation south of the Elk Hills oil field. Six hundred fifty wells with geophysical log data were used to correlate the Amnicola and Tulare Clay horizons across Elk Hills and into the adjacent Railroad Gap, Asphalto, and Buena Vista oil fields to the west and south. These correlations were used to map the structure, thickness and regional extent of the clays.

The structure map reveals a single northwest-trending anticline in the Elk Hills area. The isochore map shows that the Amnicola clay thins across the structure, but is present over the crest of the anticline. The presence of the Amnicola Clay over the crest of structural and topographic highs in the area of the Elk Hills oilfield demonstrates that the Elk Hills were covered by a paleo lake and most of the recent structural and topographic growth occurred after the deposition of the Amnicola clay.

The Tulare Clay does not extend over the structural high, demonstrating that significant structural growth occurred at Elk Hills before the deposition of the Tulare Clay, which lies below the Corcoran Clay. Based on the Amnicola Clay's assigned age of 2.2 Ma and the Corcoran Clay's age of 0.64 to 0.8 Ma, it is concluded that rapid structural growth and topographic development of the anticline at Elk Hills occurred after 2.2 Ma but before the Corcoran Clay's deposition at approximately of 0.8-0.64 Ma.

Introduction

The San Joaquin Basin is the southern part of the 700 km long by 100 km wide Great Valley of California which is an asymmetric trough filled with Mesozoic and Cenozoic sediments up to 9 km thick (Bartow, 1991). The San Joaquin Valley is surrounded by the Temblor Range to the west, the San Emigdio and Tehachapi Mountains to the south and the Sierra Nevada mountain range to the east (Figure 1) (Maher et al., 1975; Lillis and Magoon, 2008). The San Joaquin is separated from the Sacramento Valley by the positive transverse feature called the Stockton Arch that likely formed late in the Cretaceous or Paleocene and experienced uplift during the Oligocene (Bartow, 1991; Maher et al., 1975). Farther south near Bakersfield, the Bakersfield arch forms a southwest plunging structural high that separates the southern San Joaquin Basin into the Buttonwillow and Maricopa sub-basins.

The Elk Hills form a topographic high rising approximately 300 m (1000 feet) above the valley floor southwest of the Bakersfield Arch. The Elk Hills are the topographic expression of a large anticlinal structure which folds strata as young as the Pleistocene age Tulare Formation. The Upper and Lower members of the nonmarine Tulare Formation at Elk Hills are separated by a clay containing the fossil remains of the gastropod Amnicola (Maher et. al., 1975). The "Amnicola Clay" layer was deposited approximately 2.2 Ma (Miller, 1999) in a lacustrine setting. A younger clay layer within the upper part of the Tulare Formation, the Tulare Clay, was deposited before the San Joaquin Basin was covered by Corcoran Lake 0.64-0.8 Ma (Sarna-Wojcicki, 1976; Kiser et al., 1988; Bartow, 1991;McPherson and Miller, 1990). Three dimensional seismic data indicate that the Tulare Clay may be equivalent to the Basal Alluvial

Clay of Kiser et al. (1988) (Eric Greenwood, California Resource Corporation, personal communication).

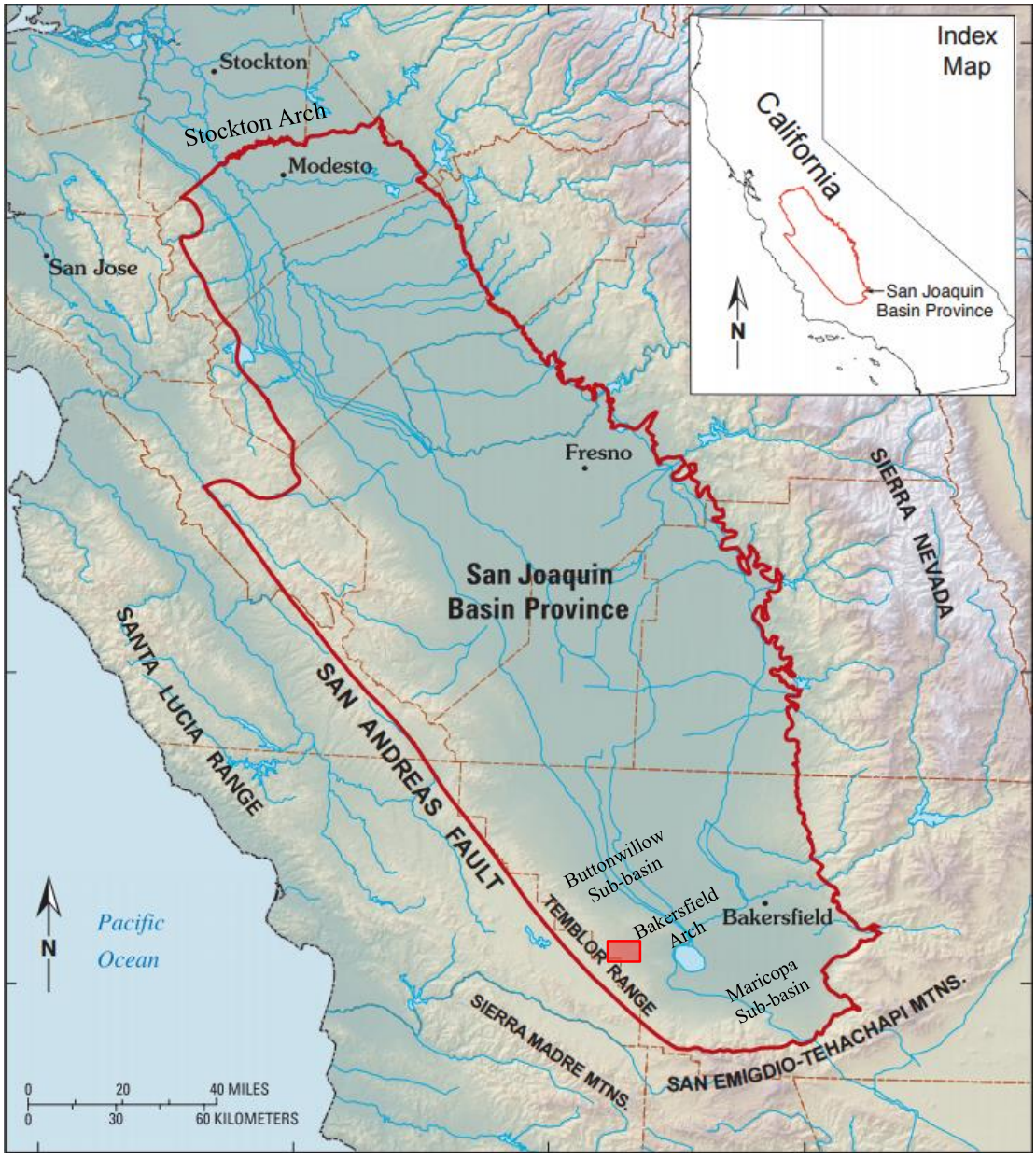

Figure 1. Regional map of the San Joaquin Basin with the study area highlighted in red (modified from Lillis and Magoon, 2008).

By utilizing electric well logs for correlation in the Elk Hills, Asphalto, and Railroad Gap oil fields, the regional extent of "Lake Amnicola" and Lake Tulare can be determined for this area. It is especially important to determine if the Amnicola clay extends over the crest of the Elk Hills anticline. If so, the area occupied today by this topographic and structural high was originally covered by the paleo lake and significant uplift forming the present day topographic high occurred after deposition of the Amnicola Clay. If the Amnicola clay layer is not present on the structurally high portions of the anticline it would indicate that Elk Hills was an "island" in the "Amnicola lake" and that significant growth of the structures took place prior to, or shortly after, the deposition of the Amnicola clay.

Regional Geology

The San Joaquin Basin initially developed as a forearc basin that originated during the Mesozoic. During this time the Farallon plate was being obliquely subducted eastward under the North American plate resulting in arc magmatism in the Sierra Nevada mountain range (Bartow, 1991; DeCelles, 1998). The San Andreas Fault system became active approximately 30 Ma as a result of the ancestral East Pacific rise encountering the subduction zone. This event is hypothesized to have caused uplift and faulting in the southern San Joaquin basin (Atwater, 1970; Bartow, 1991; Dickinson and Seely, 1979). This transition resulted in the eventual closing of the basin to the Pacific Ocean as highlands of granitic basement were transported approximately 320 km north along the San Andreas Fault system (Graham et al., 1989).

Elk Hills is located in the southwestern part of the San Joaquin Basin, 40 miles southwest of Bakersfield (Figure 1). To the west, south and east of the Elk Hills oil field lies the Railroad Gap, Asphalto, Buena Vista, North and South Coles Levee oil fields (Figure 2).

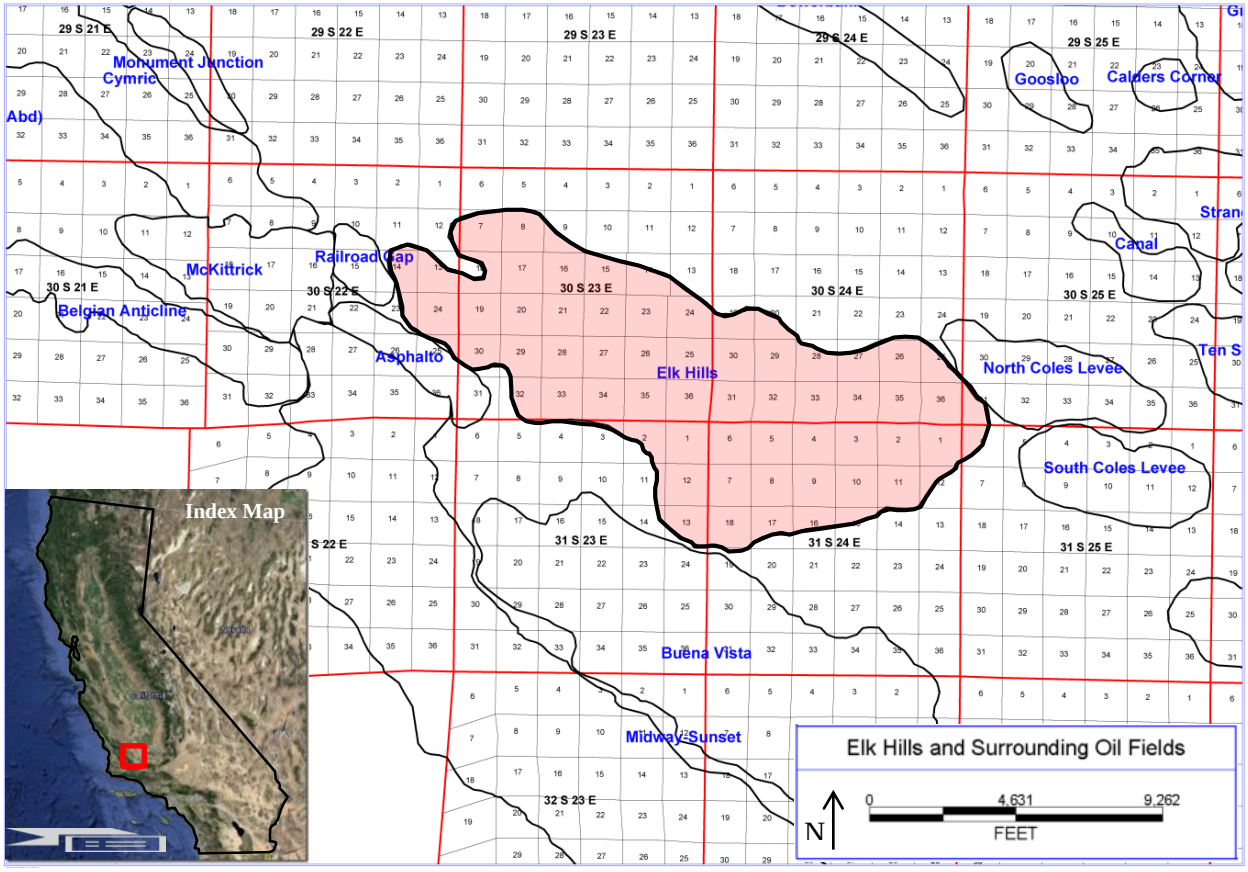

Figure 2. Location map of Elk Hills and surrounding oil fields in the southern San Joaquin Basin. Study area outlined by a red box on index map.

The Elk Hills rise up to 305m (1000ft) above the valley floor (Maher et al, 1975; Reid and McIntyre, 2001) and are the surface expression of an anticlinal structure (Figure 3). The first producing oil well was drilled in 1911 to a depth of 1219m (4,000ft) (Pemberton, 1929).

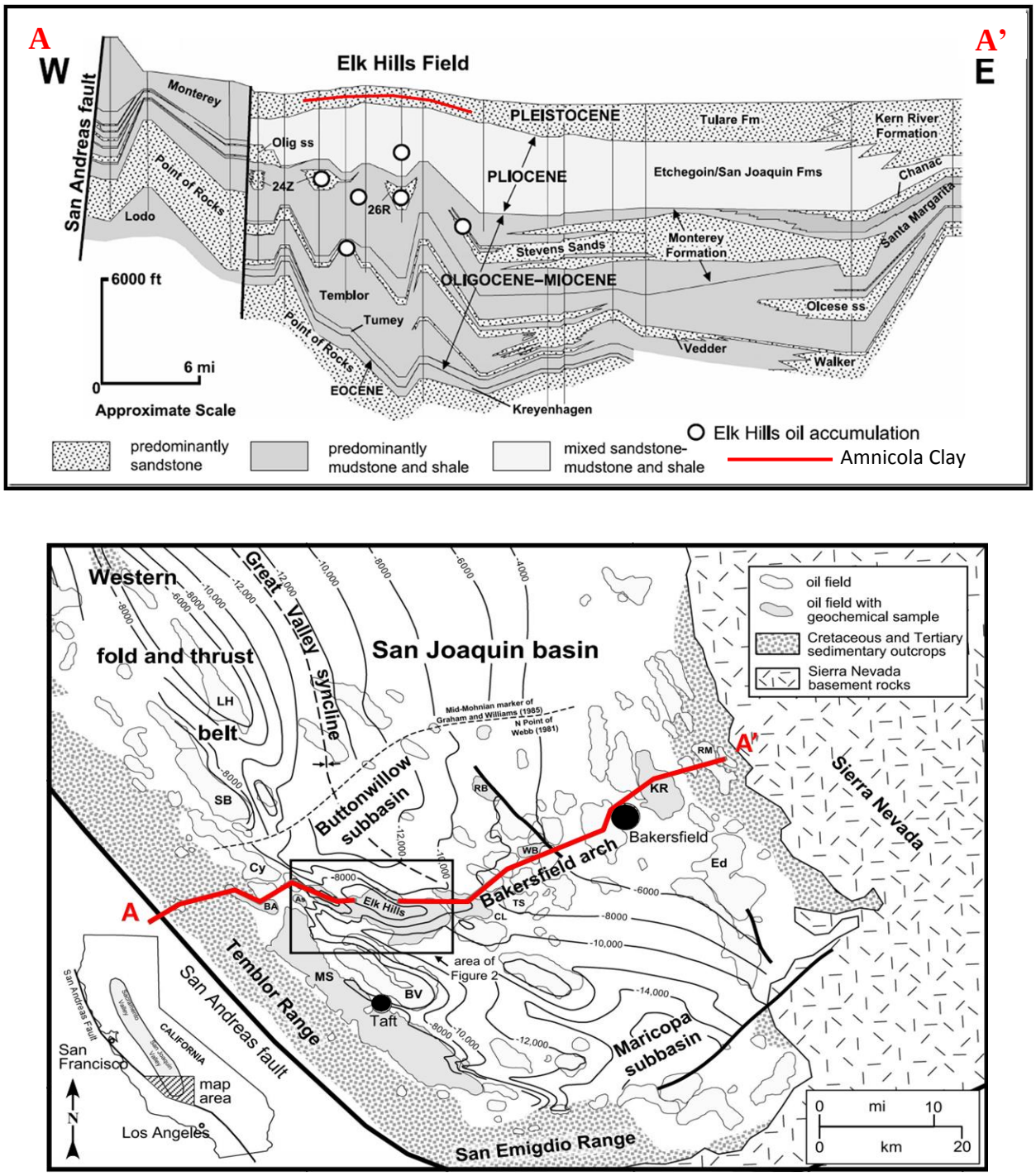

Figure 3. A generalized west -east cross section in the southern San Joaquin basin through the Elk Hills oil field noted on cross section location map. The Amnicola Clay contained within the Pleistocene aged Tulare Formation is highlighted in red (modified from Zumberge et al., 2005).

While the surface expression of Elk Hills is that of a single northwest-trending , doubly-plunging anticline, three northwest-southeast elongated domes are present in the subsurface: the 29R, 31S and the Northwest Stevens anticlines (Zumberge et al., 2005; Cobos, 2006). The Elk Hills lie at the southern boundary of the west side fold belt that is comprised of northwest-trending faults and folds east of the San Andreas Fault (Bartow, 1991). The anticlines formed in response to north and northeast directed compression at high angles to the San Andreas fault system. Mechanical modeling performed by Fiore et al. (2007) show that structure growth at Elk Hills was due to thrust faulting as a result of northeast-southwest compression. Folding started in the Miocene, increased during the Pliocene, and is still active today (Harding, 1976; Zumberge et al., 2005; Cobos, 2006).

Sediment deposition in the Elk Hills area was controlled by a series of tectonic events as western California transitioned from a forearc to a transform basin. Predating closure of the basin to the Pacific Ocean, deposition consisted of shallow and deep marine sand and clay deposits of the Temblor Formation in the Oligocene (Figure 4) (Reid, 1995). During middle to late Miocene time the basin transitioned to deep water clay, turbidite and diatomite deposits of the Monterey Formation after movement on the San Andreas Fault partially cut off the basin from the Pacific Ocean (Reid, 1995).

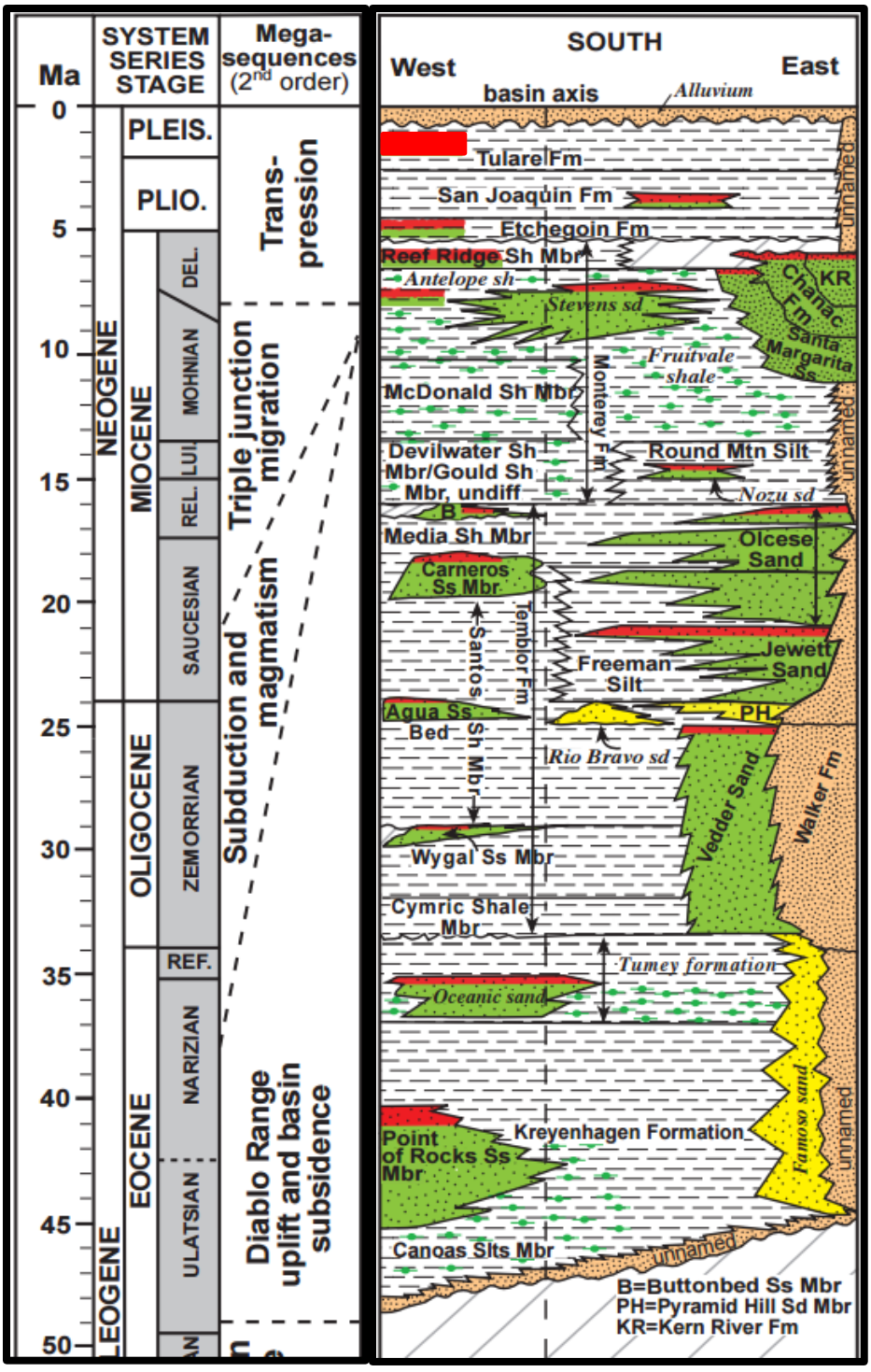

Figure 4. Stratigraphic column for the San Joaquin Basin. The Amnicola Clay is represented by the red colored box with in the Plio-Pleistocene aged Tulare Formation (Modified from Lillis and Magoon, 2008).

During Pliocene time increased sedimentation rates were associated with the uplift of the Sierra Nevada, Temblor, and San Emigdio Ranges and the basin transitioned from deep marine to nonmarine. The Etchegoin Formation was deposited in a tidal to shallow marine environment around 5.3 mya followed by the San Joaquin Formation, which is a mix of marine, brackish, and freshwater sediments deposited at or near sea level in tidal flat and channel environments (Bartow, 1991; Reid, 1995).

Alluvial fans of the Plio-Pleistocene aged Tulare Formation expanded across the San Joaquin formation towards the basin center, and by 3 mya, deposition occurred in fluviodeltaic, alluvial fan, and lake settings (Figure 5) (Reid, 1995; Miller, 1999).

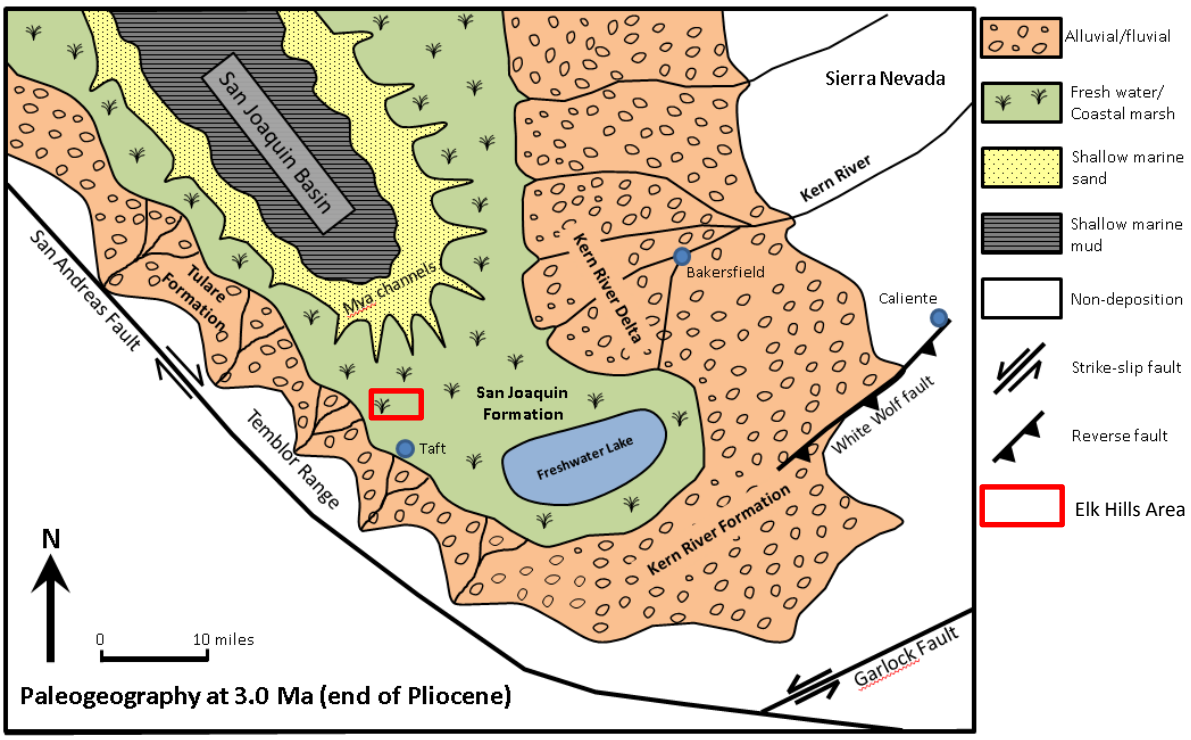

Figure 5. Depositional environment and paleogeography of the southern San Joaquin basin at the end of the Pliocene. The Elk Hills Area, outlined in red, is dominated by lake and river deposits (modified from Reid, 1995).

Named by Anderson (1905), the Tulare Formation was described as strata exposed in Kettleman Hills near Tulare Lake, where it consists of nonmarine sandstones, conglomerates and mudstones (Maher et al., 1975). Arnold and Johnson (1910) mapped the Tulare equivalent strata in the Elk Hills area, originally naming it the McKittrick Formation until Gester (1917) renamed it the Tulare Formation in 1917 (Maher et al., 1975).

The Tulare Formation at Elk Hills, and in the surrounding Asphalto and Rail Road Gap oil fields can be separated into three members; a upper sandstone and conglomerate, an underlying mud stone, and a lower sandstone and conglomerate (Maher et al., 1975). According to Maher et al. (1975) the lower member is composed of an olive-gray, poorly consolidated, very fine to very coarse grained sandstone containing feldspathic pyrite and biotite. The upper member of the Tulare Formation is made up of unconsolidated feldspathic medium to very coarse grained sandstone (Maher et al., 1975). In the upper Tulare Formation it is common to see unsaturated "air sands" with the characteristic "cross over" response of the neutron-density log. The clay separating the sandstone members is an olive gray, partly calcareous/dolomitic, claystone that contains the gastropod *Amnicola* (Figure 6) (Woodring et al., 1932; Berryman, 1973; Maher et al., 1975).

Figure 6. Photograph of the gastropod *Amnicola longinqua* found within the Amnicola Clay layer (http://inyo.coffeecup.com/site/kh/tularefm4.html, accessed 10/19/2015)

Age determination for the Tulare Formation is constrained using biostratigraphy and radiometric methods. The age for the base of the Tulare formation has a range from 3.4-2.2 Ma. The date of 3.4 Ma comes from age of the Putah Tuff at the base of the Tulare at Kettleleman Hills and the 2.2 Ma date was determined from a tephra layer also found at the base of the lower Tulare in Kettleman Hills (Miller, 1999). Above the Tulare Clay, the Corcoran clay layer, a lacustrine clay within the upper Tulare Formation has been dated at approximately 0.64 Ma, based on the age of the overlying Friant Pumice Member in the axis of the San Joaquin Valley (Page, 1983; Bartow, 1991; Miller, 1999).

Miller (1999) noted three large lacustrine flooding events within the Tulare Formation that are visible in seismic (Figure 7). The deepest flooding event, the Blue Horizon (Figure 7), is dated at approximately 3.4 Ma based on the Putah Tuff and corresponds to the upper San Joaquin Formation (Miller, 1999).

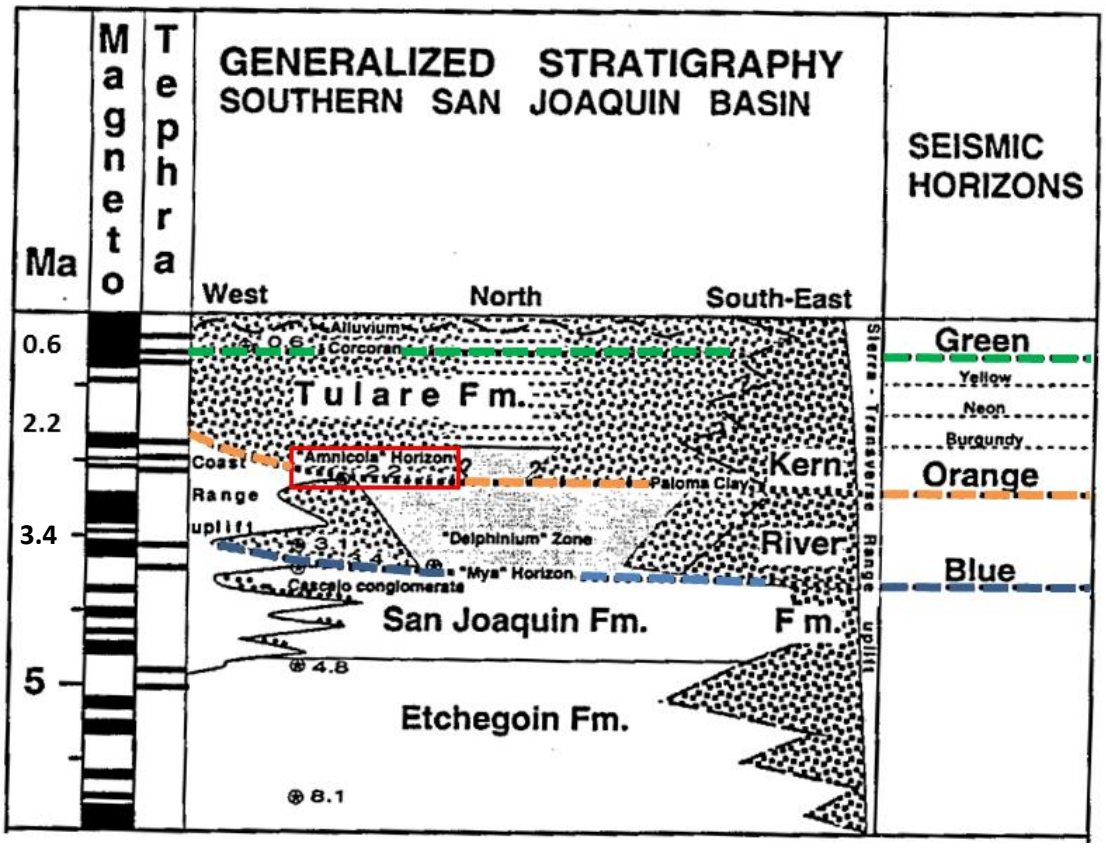

Figure 7. Generalized Stratigraphy of the Southern San Joaquin Basin with Miller's (1999) Blue (3.4 Ma), Orange (2.2 Ma) and Green (0.64 Ma) seismic flooding horizons. Zone containing the Amnicola Clay highlighted in red (Modified from Miller, 1999)

The Orange Horizon represents the Amnicola lacustrine flooding event that occurred at Elk Hills and is dated at 2.2 Ma based on tephra data from Kettleman Hills (Miller, 1999). The Green horizon represents the Corcoran Clay dated at 0.64-0.8 Ma (Figure 7) (Miller, 1999). The three seismic horizons are traced to Elks Hills in Seismic Line 133 (Figure 8) (Miller, 1999).

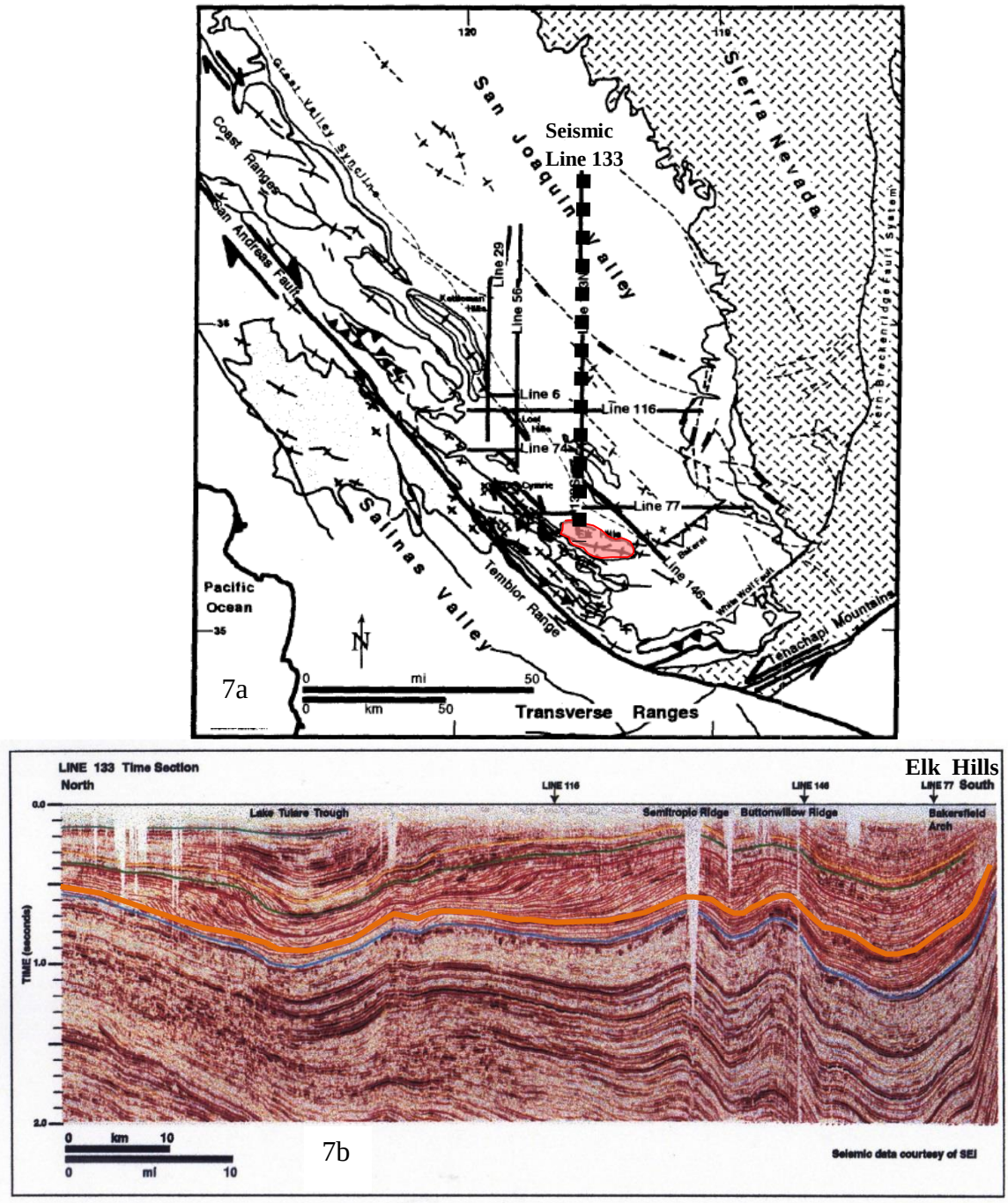

Figure 8. (a).. Location of seismic lines used by Miller (1999) to correlate flooding event horizons in the Elk Hills area. Seismic line 133 is highlighted in black intersecting the Elk Hills oil field highlighted in red. (b). The Green, Orange and Blue flooding events as described by Miller (1999). The Amnicola flooding event corresponds to the Orange horizon (Modified from Miller, 1999).

Statement of the Problem

The Amnicola Clay is important in the Elk Hills region due to its role as a local confining layer or aquitard, which prevents saline oilfield produced waters injected into the lower part of the Tulare Formation from degrading fresh groundwater in the upper part of the Tulare Formation (Crosby and Schymiczek, 1990). The presence of the confining clay layer is an important consideration in order to qualify for aquifer exemption status in response to California Senate Bill 4 approved September 20, 2013 (the Well Stimulation or so-called "fracking" bill).

In order to obtain an aquifer exemption for the Tulare reservoir at Railroad Gap and Asphalto it is necessary to prove that the Tulare is not currently, nor would be in the future, a source of usable water for domestic, urban, or agricultural purposes. The US EPA defines an Underground Source of Drinking Water (USDW) as "An aquifer or portion of an aquifer that supplies any public water system or that contains a sufficient quantity of ground water to supply a public water system, and currently supplies drinking water for human consumption, or that contains fewer than 10,000 mg/l total dissolved solids and is not an exempted aquifer." (http://water.epa.gov/type/groundwater/uic/glossary.cfm#t, accessed 12/29/2014).

In a multi-step process, the Division of Oil, Gas, and Geothermal Resources (CA DOGGR) must agree with the entity applying for the exemption, then submit the report to the State Water Resources Control Board who then will submit the recommendation to the US Environmental Protection Agency (US EPA). This federal agency has the final authority on aquifer exemptions. The US EPA allows for industrial waste, oil and gas, and mine related injection into exempted aquifers through the Underground Injection Control Program, which defines these operations as Class I, II, or III, respectively (http://yosemite.epa.gov/r10/water.nsf/uic/uic+program, accessed 10/19/2015). In order to qualify as an exempted aquifer under US EPA rules, the aquifer must meet the following

requirements as per regulation 40 CFR 146.4 (http://www.gpo.gov/fdsys/granule/CFR-2011-title40-vol23/CFR-2011-title40-vol23-sec146-4, accessed 12/29/2014):

(a) The aquifer does not currently serve as a source of drinking water; and

(b) The aquifer cannot now and will not in the future serve as a source of drinking water because:

a. It is mineral, hydrocarbon or geothermal energy producing, or can be demonstrated by a permit applicant as part of a permit application for a Class II or III operation to contain minerals or hydrocarbons that considering their quantity and location are expected to be commercially producible.

b. It is situated at a depth or location, which makes recovery of water for drinking water purposes economically or technologically impractical;

c. It is so contaminated that it would be economically or technologically impractical to render that water fit for human consumption; or \

d. It is located over a Class III well mining area subject to subsidence or catastrophic collapse; or

(c) The total dissolved solids content of the ground water is more than 3,000 and less than 10,000 mg/l and it is not reasonably expected to supply a public water system.

Mapping the thickness and lateral extent of the Amnicola Clay will determine if there is vertical confinement within the Tulare Formation, which is an important requirement for the aquifer exemption process.

Methods

Of the 3,114 wells with geophysical log data, 650 were selected for this mapping project (Figure 9) and the Amnicola and Tulare Clay horizons were correlated throughout the Elk Hills field and surrounding areas (Figure 9). No digitized well logs were available for this project so mapping and correlation was performed on raster image logs provided by the State of California Department of Conservation Oil, Gas, and Geothermal (DOGGR, http://www.conservation.ca.gov, accessed 1/1/2014), and by the subscription-based service, TGS Log Line™.

Log correlation and mapping were conducted using the software Petra™ by IHS. All image files were loaded into Petra™, depth registered, and straightened if needed. For type log displays and cross sections, selected raster image logs were digitized using Petra™ . Each well with a raster image log was studied to see if the well was logged at shallow enough depths to potentially contain a record of the Amnicola Clay.

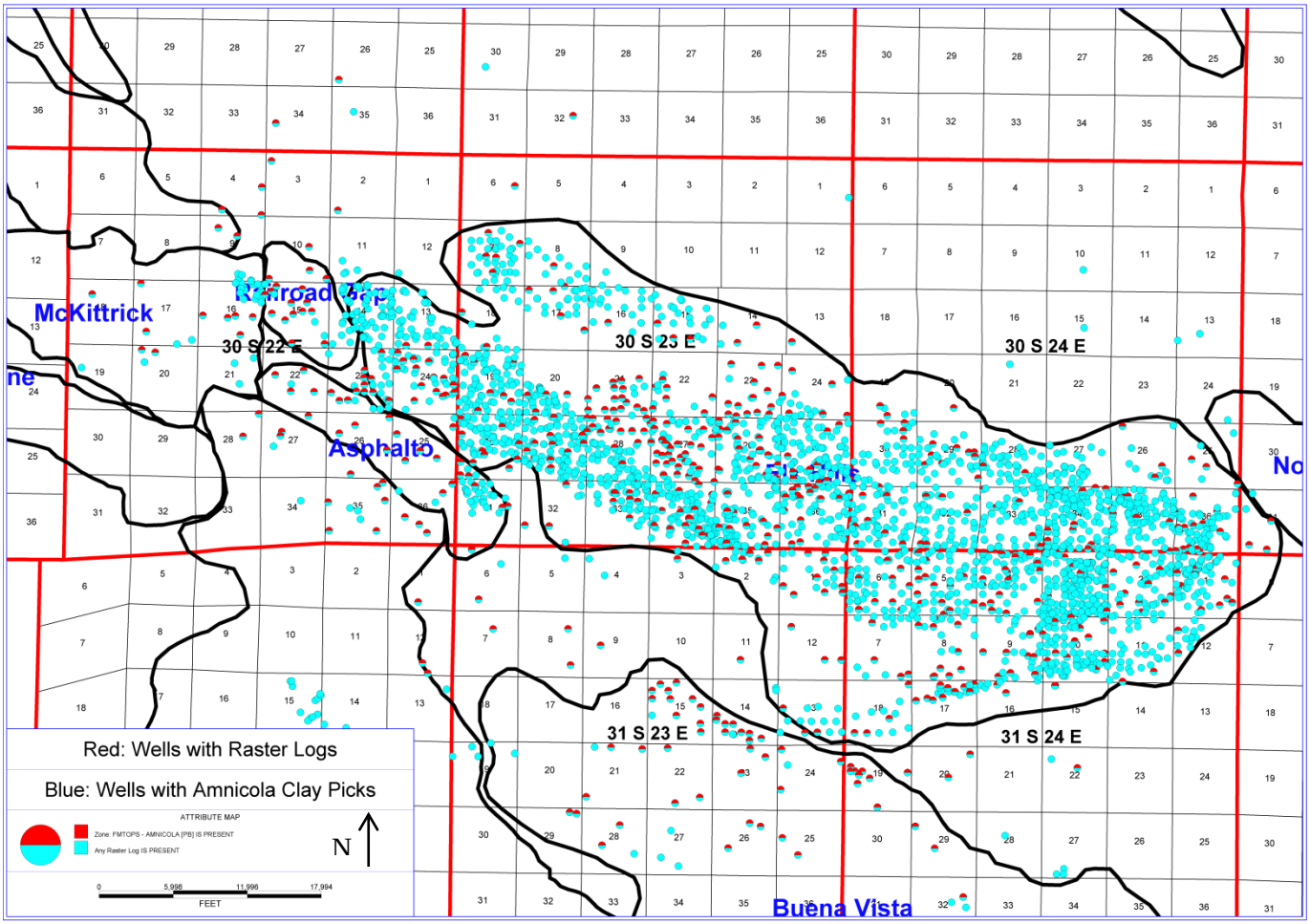

Figure 9. Regional map displaying the 3,114 wells with raster image electric logs highlighted in blue potentially contained the Amnicola Clay. 650 wells highlighted in red were used to construct structure and isopach maps in Petra™.

Well control on the Amnicola Clay is particularly good in section 27 of Township 30S Range 23E where the lower Tulare Formation is used for wastewater injection and has many shallow logs through the Tulare Formation. The type log (Elk Hills 42WD-28R; Figure 10) is located in this section and the log signature was used to correlate across the Amnicola Clay across the field.

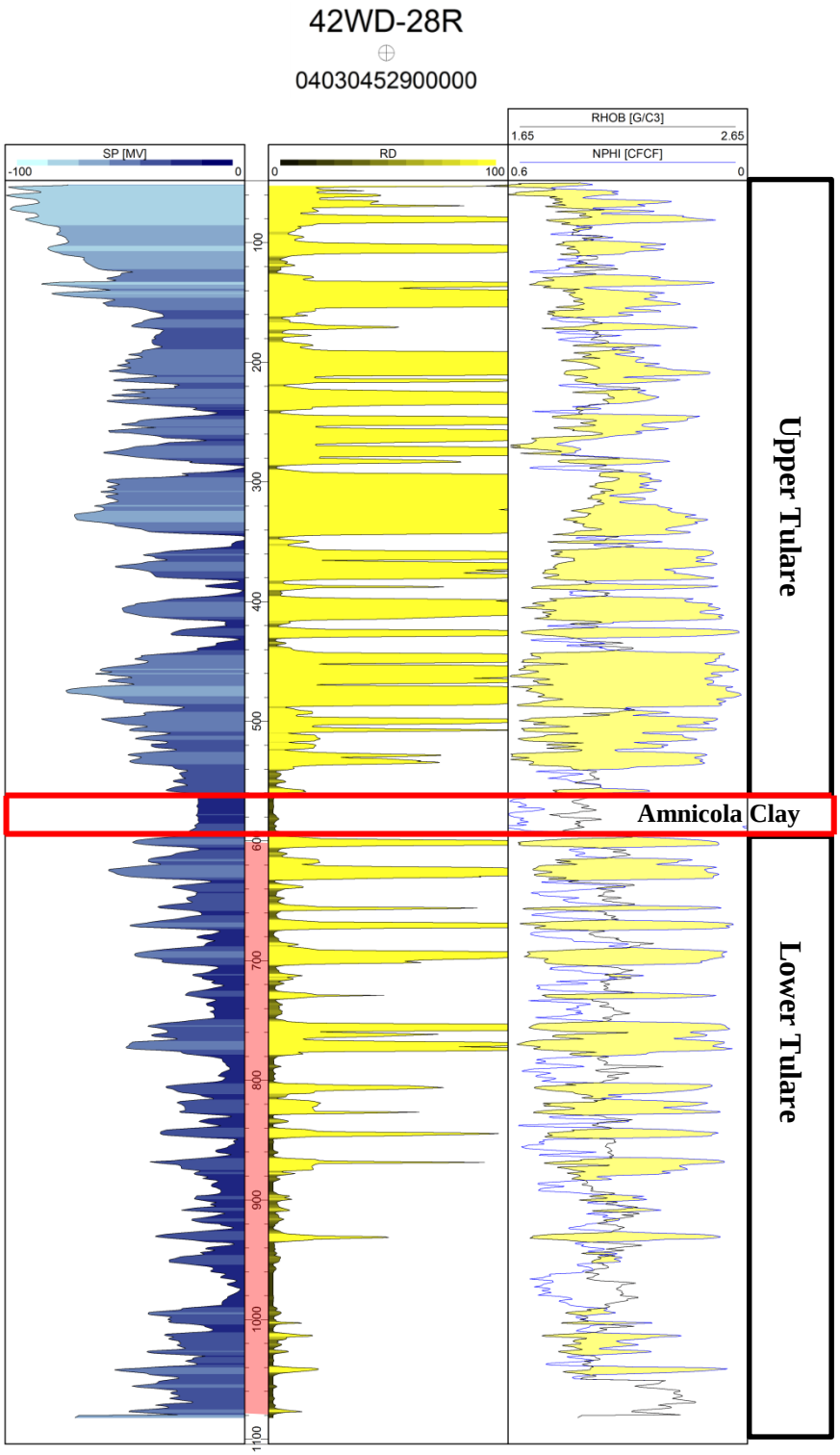

Figure 10. Type log for the Amnicola Clay. Water disposal well 42WD-28R from T30S R23E Section 28.Left track shows SP, center track shows deep resistivity and the right track has neutron porosity and bulk density with cross-over response in yellow. The perforated interval is highlighted in red on the depth track and the Amnicola Clay is outlined by the red box.

The spontaneous potential (SP) and resistivity electric log curves were most commonly used to correlate the Amnicola Clay. The SP curve measures the naturally-occurring electric potential between the well bore fluid and the fluid in the surrounding formation and is related to the permeability of the formation and the salinity of the fluids (Hilchie, 1979). For permeable zones, in an environment in which the drilling fluid is fresher than the formation fluid, the SP kicks to the left (negative), while in a zone with lower permeability or very fresh formation water, the SP kicks right (positive) from a shale baseline (Hilchie, 1979).

Resistivity logs were also used to identify the Amnicola Clay. Resistivity logs measure the formations' ability to conduct an electrical current. In the case of most clays, electrical current can be transmitted, so they have a low resistivity reading. Zones with low resistivity (conductive) paired with positive SP values indicate the presence of clays, including the Amnicola Clay, in the study area.

Some of the more recent electric logs contain neutron porosity and density porosity logs in addition to SP and resistivity. The neutron log determines porosity by measuring the abundance of hydrogen atoms in the formation. Hydrogen atoms are usually associated with formation fluids (water and liquid hydrocarbons) in the pore space. The density log measures porosity as the electron density opposite the wellbore. Fluids have a lower electron density than the rock matrix and an abundance of fluid corresponds to higher porosity. The neutron porosity curve in the Amnicola Clay reads incorrectly high porosity values due to the presence of OH^- groups attached to the clay minerals. Neutron porosity values often read above 60% (go off scale to the left) if the log scale is set between 60% and 0% (Figure 10). The sands above and below the Amnicola Clay often show the neutron porosity curves reading lower values than the density

porosity curve- a phenomenon known as gas cross-over effect-due to the fact that the sands lie within the air-filled vadose zone above the regional water table. In these cases the Amnicola Clay is more distinctive as the clay zone does not exhibit cross-over effect (Figure 10).

Results

The structure map showing the elevation of the top of the Amnicola Clay relative to sea level exhibits a single northwest trending anticlinal structure (Figure 11) in the Elk Hills field as opposed to the three anticlinal structures exhibited in maps of Pliocene and older formations noted by Cobos (2006). Higher elevations appear yellow and lower appear blue and purple. The structurally highest elevation is 305m (1000ft) above sea level in Sections 28 and 29, T30S R23E. The lowest elevation data point along the northeastern flank of the structure is at 618m (2,029ft) below sea level, in section 32, T29S R 23E. The southwest flank of the structure dips southwest towards the Buena Vista lakebed beyond which the dip reverses to form the northeast flank of the northern anticline in the adjacent Buena Vista oil field. The lowest correlated elevation of the Amnicola Clay is located southeast of the Elk Hills field in the Buena Vista Lake bed at a depth of -629m (-2065ft) (Figure 11). This results in 923m (3028ft) of structural relief. Four northeast-southwest trending and one west-east trending cross section across the study area display the anticlinal structure of the Amnicola Clay (Figure 12, Appendix 1-7).

An isochore map was created over the study area (Figure 13) using picks from the top and base of the Amnicola Clay. The resulting map shows the changes in clay thickness, which generally ranges from 15-80 feet. The thickness is shown by color with orange and red colors representing thicker intervals and blue and purples representing thinner areas. The structural contours are plotted on top to display the relationship between elevation and thickness trends.

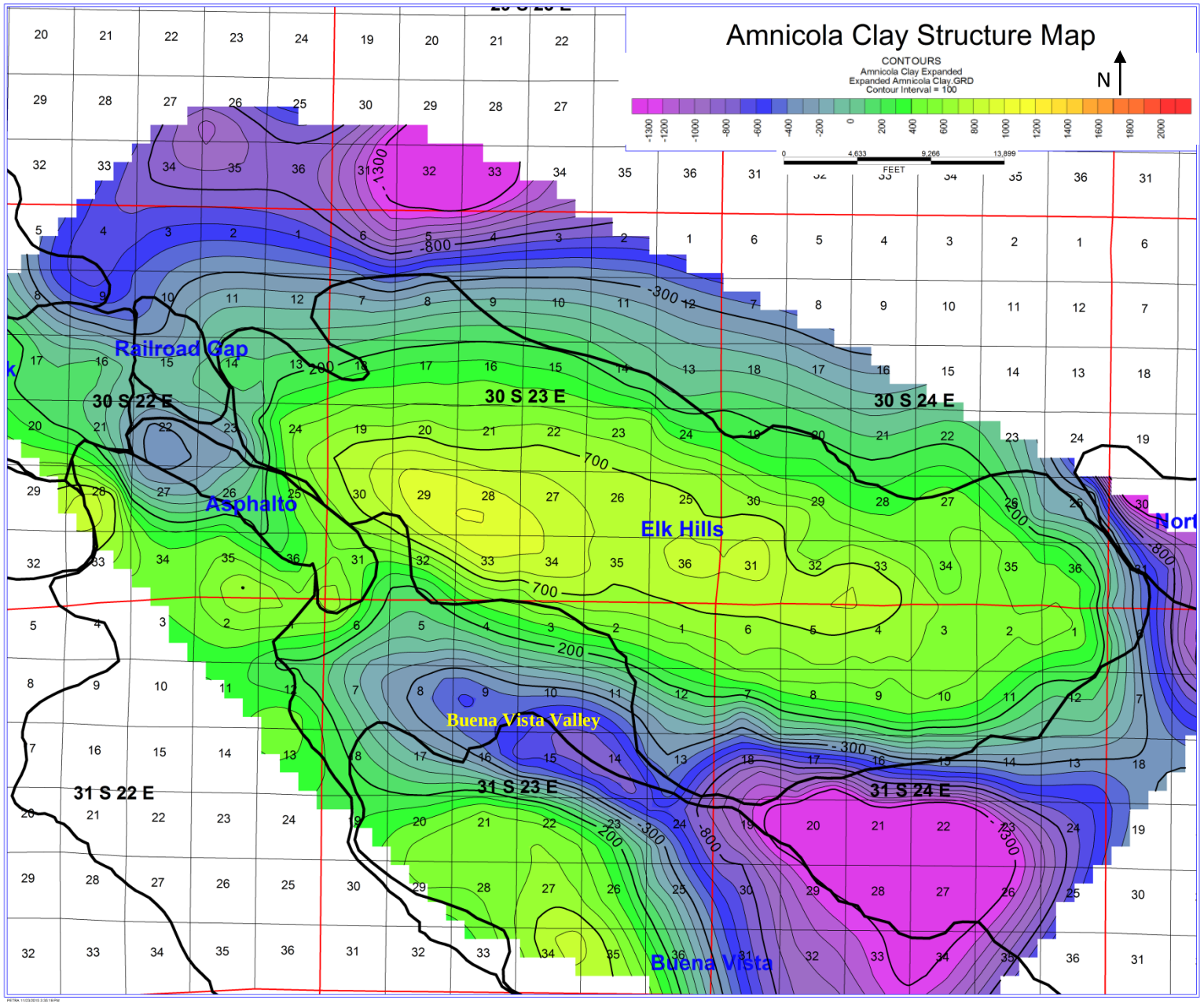

Figure 11. Structure map of the Amnicola Clay forming a single northwest trending anticline. Higher elevations appear yellow and lower appear blue and purple.

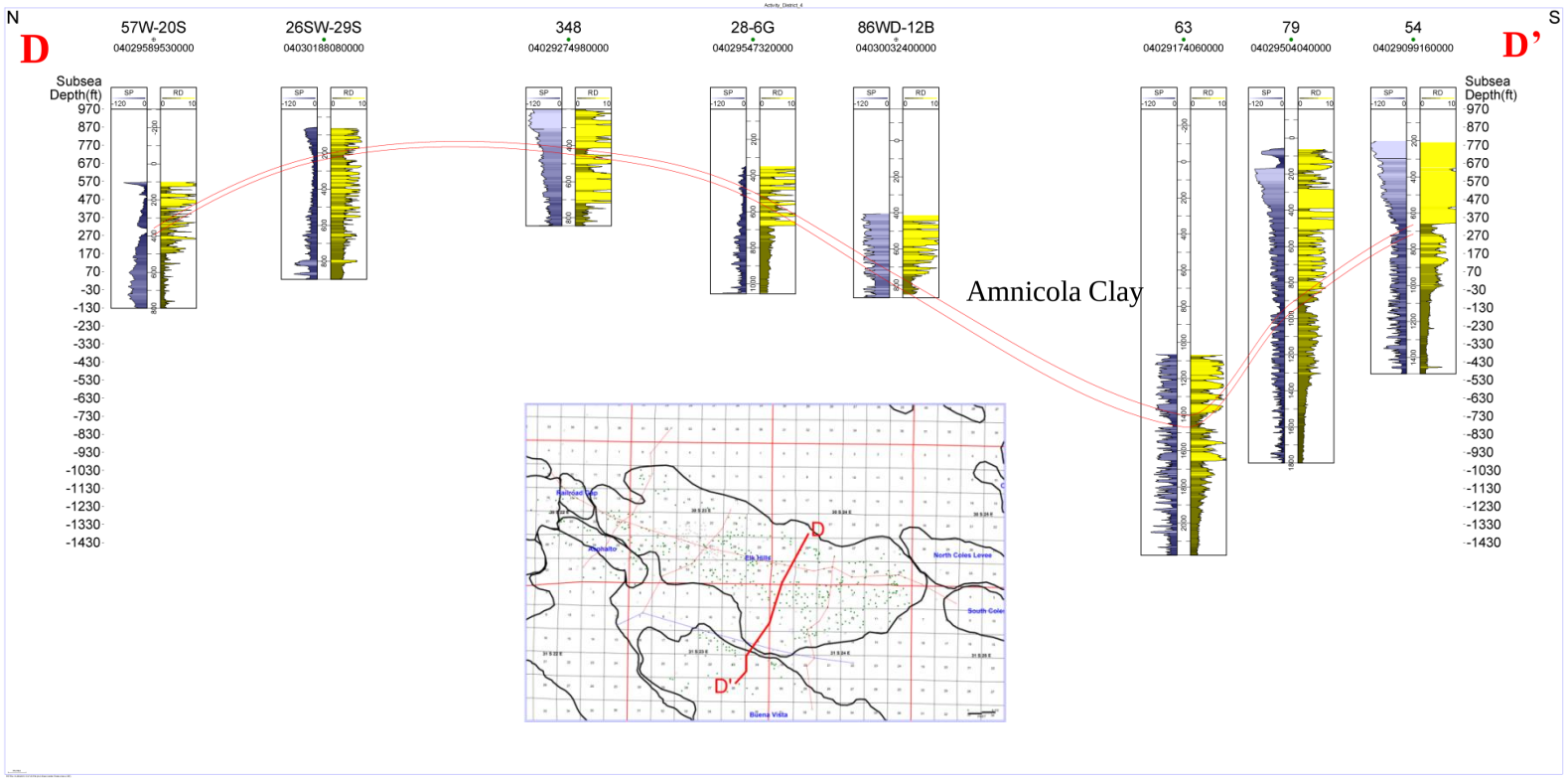

Figure 12. Northeast to southwest cross section D-D' showing structure on top of the Amnicola Clay (Outlines in red).

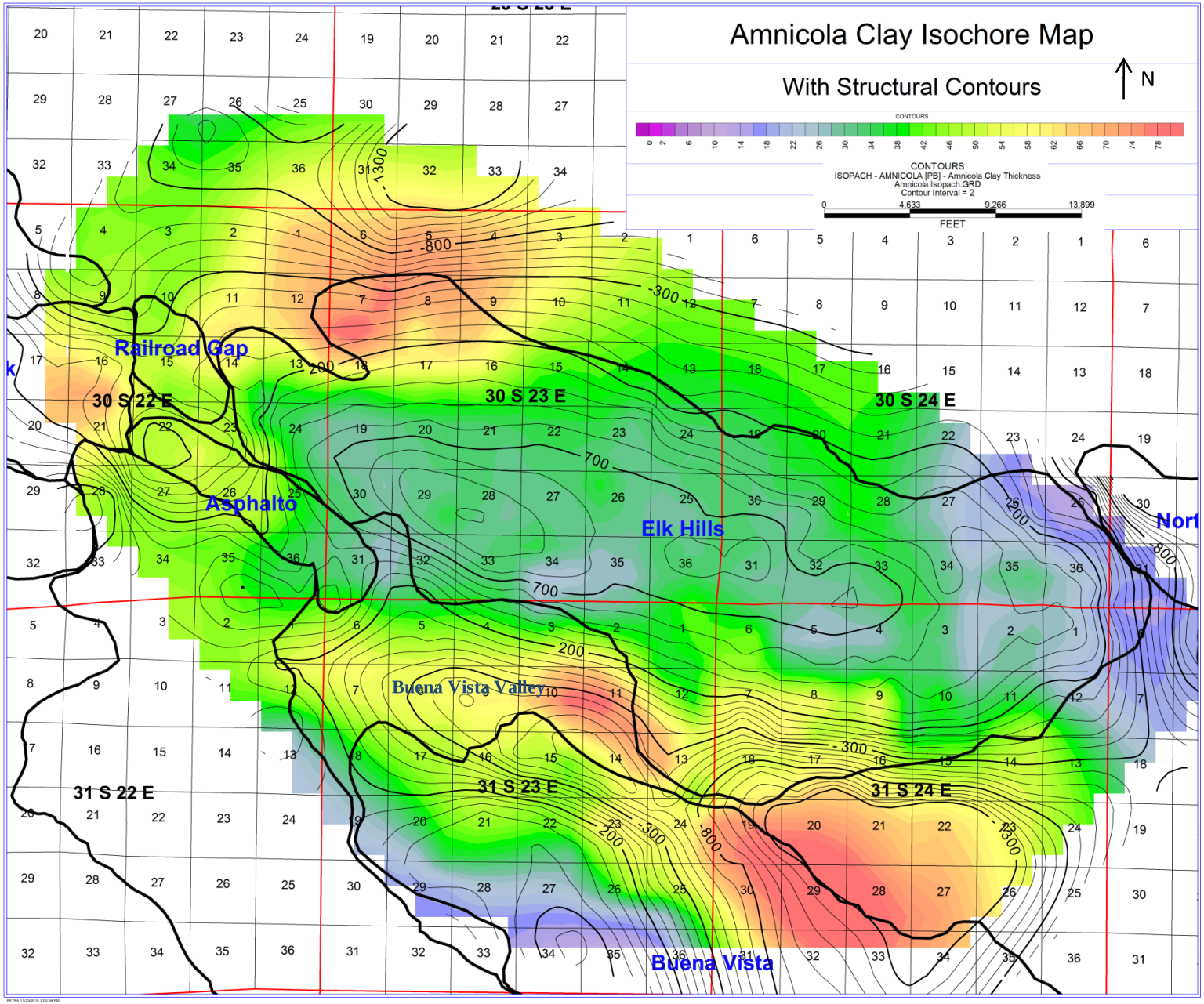

Figure 13. Amnicola Clay isochore map overlain on the structural contour map. Red areas indicate thicker intervals while blue indicate thinner.

The general trend of the thickness map demonstrates that the Amnicola Clay is thinner over the structural highs and thickens in structural lows. The clay reaches its maximum thickness to the southeast in the Buena Vista lakebed.

While correlating the Amnicola Clay south of the Elk Hills field, a second clay interval was discovered at a shallower depth (Figure 14). This clay is labeled as the "Tulare Clay" on some electric logs and in well histories found on the DOGGR website (http://www.conservation.ca.gov/dog/Pages/Index.aspx; Accessed 1/1/2015). In this clay interval, the electric log shows a low resistivity value that increases up-section corresponding to a coarsening up sequence (Figure 14) common in prograding delta deposits (Negrini et al., 2009). The clay is located the southern part of the Bakersfield Arch and dips and thickens southwest towards the Buena Vista Lakebed. A west to east cross section (Figure 15a) (Appendix 4) and a north to south cross section (Figure 15b) (Appendix 5) demonstrate the structural and thickness changes exhibited by the Tulare clay. The Tulare Clay dips towards the southwest (Figure 16) and appears to pinch out to the north, south and west of the Buena Vista Valley (Figure 17) and thicken into the Buena Vista Lake Bed to the east.

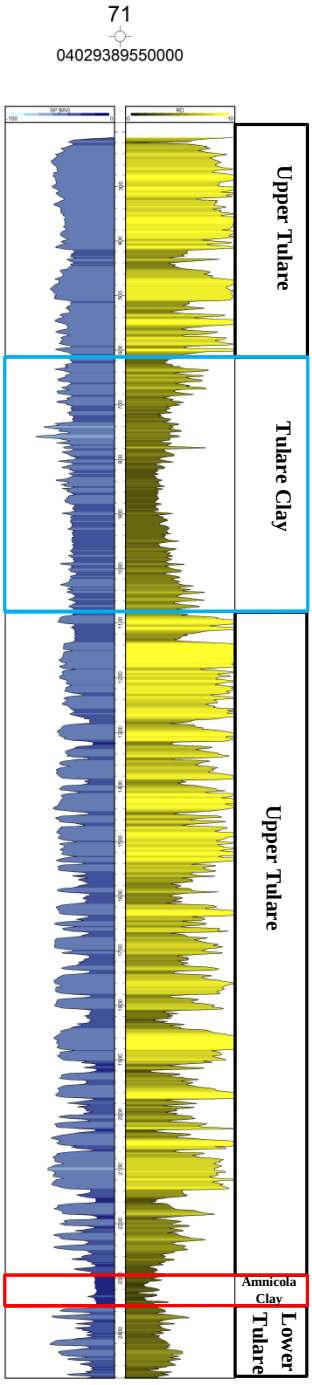

Figure 14. Type log for the Tulare Clay (blue). The Amnicola Clay is shown in red for reference. The Tulare Clay lies within the upper Tulare Formation. Well number 71 (API number 04029389550000), located in Section 20 of T31S R24E, (DOGGR, http://owr.conservation.ca.gov/, accessed 1/1/2015).

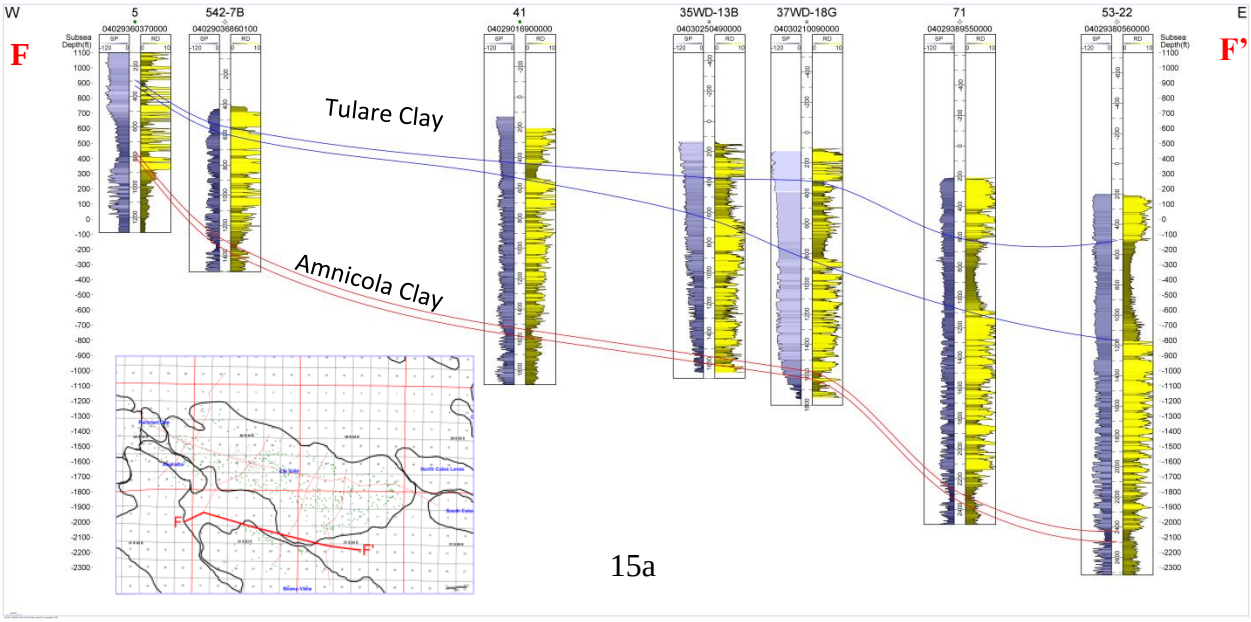

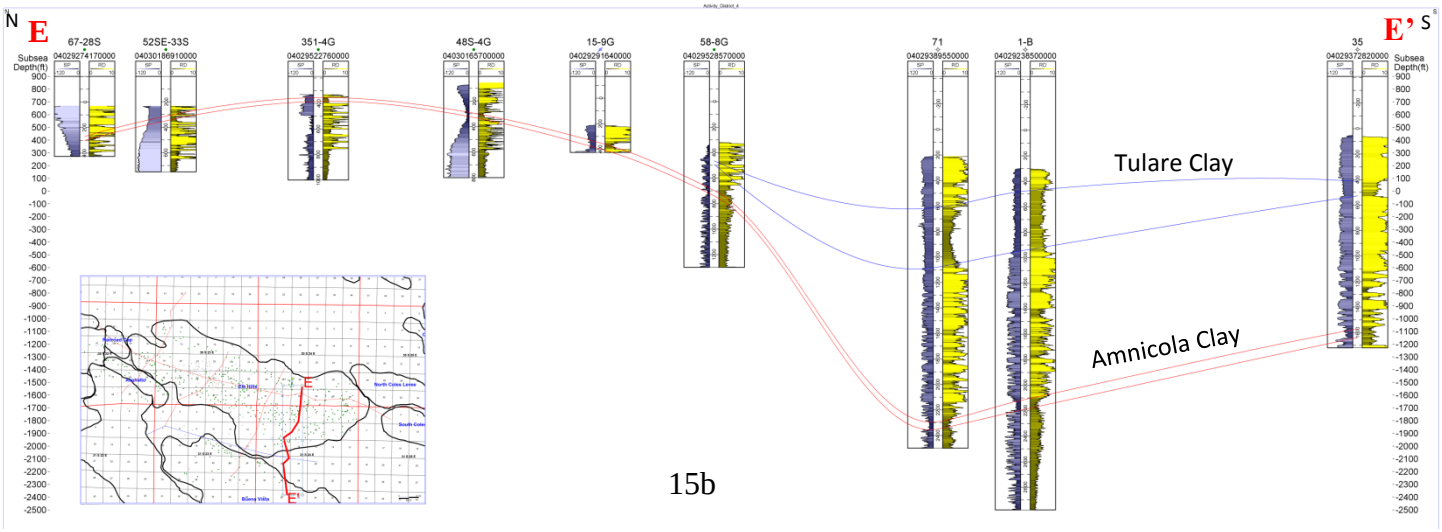

Figure 15.(a). West to east cross section F-F’ and (b). north to south cross section E-E’ showing structure on top of the Tulare Clay and Amnicola Clay.

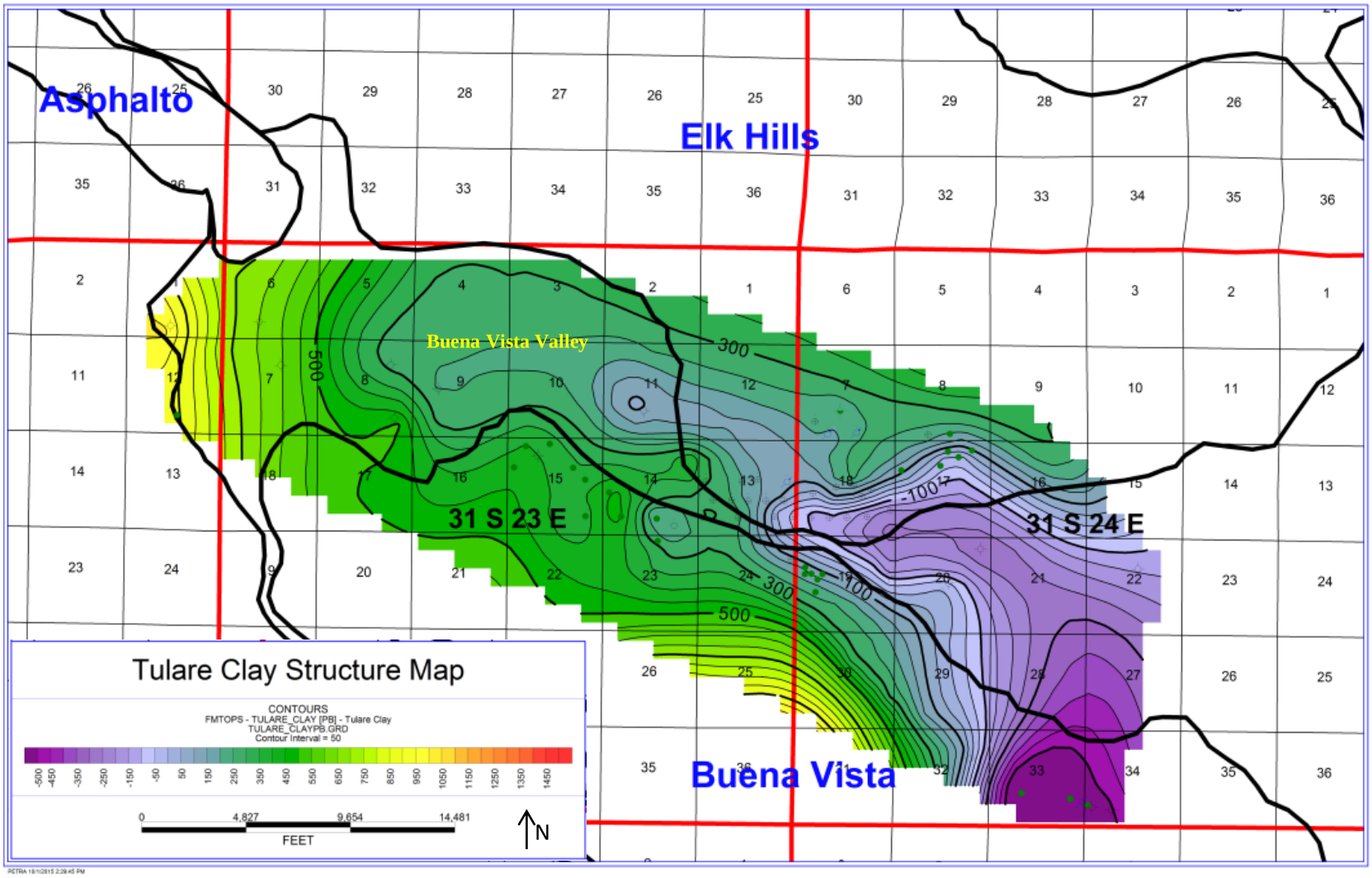

Figure 16. Structure map on top of the Tulare Clay

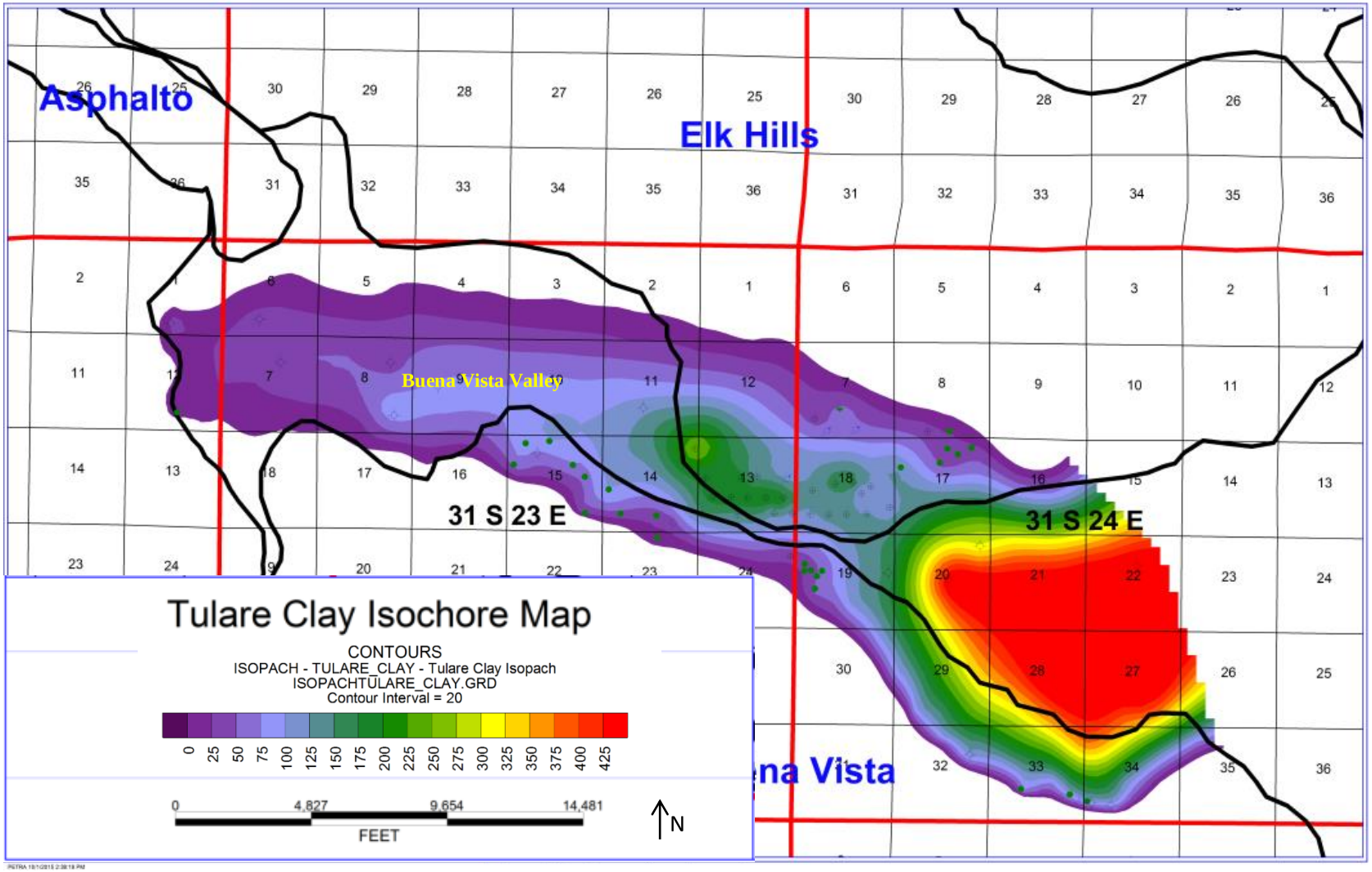

Figure 17. Isochore thickness map of the Tulare Clay.

Discussion/Conclusions

Mapping the Amnicola Clay across Elk Hills has shown there has been 923m of structural relief that occurred after 2.2 Ma and before deposition of the Tulare Clay. This late structural growth is attributed to compression on the San Andreas Fault system that caused uplift in the Temblor Range, activation of the west side fold belt and further uplifted the preexisting anticline at Elk Hills (Bartow, 1991; Reid, 1995). Thrust faulting, as proposed by Fiore et al. (2007), began around 10 Ma, but did not create a significant surface expression until after the deposition of the Amnicola Clay.

Although the Amnicola Clay is shown to thin over present-day structural highs, the clay deposit covers the entire extent of the Elk Hills anticline thus demonstrating that the structures at Elk Hills during lake high stand were not significantly high to form islands within the lake although today they stand nearly 1 km above the valley floor. This suggests that significant uplift on the Elk Hills structure was not initiated until later in the history of deposition of the Tulare Formation (Nicholson, 1990; Reid, 1990).

The clay above the Amnicola Clay in the Buena Vista Valley, south of the Elk Hills oil field, is referred to locally as the Tulare Clay on well logs and lies below the Corcoran Clay, which correlates to Miller's (1999) green horizon that is dated between 0.8- 0.64 Ma based on the Bishop ash bed and the Lava Creek ash bed (Baron et al., 2008). By the time the Tulare clay was deposited, the Elk Hills structure had grown to such a height that the clay was confined to the lower elevations of the Buena Vista Valley and the Elk Hills anticline may have formed a positive feature, or island, within the lake unless it originally covered the Elk Hills area and was removed by later erosion during uplift.

Mapping the Amnicola and Tulare Clays gives a relative timing bracket for the structural growth of the Elk Hills anticline. Evidence from well correlation shows that the Amnicola Clay extends over the Elk Hills structure and that clay is dated to approximately 2.2 Ma (Miller, 1999); thus nearly 1 km of structure relief occurred after 2.2 Ma and before the Tulare Clay was deposited. Deposition of the Tulare Clay occurred before the overlying Corcoran Clay was deposited at approximately 0.8-0.64 Ma.

The presence of the Amnicola Clay across the study area indicates a large flooding event occurred that blanketed the region with lacustrine mud. The gastropod *Amnicola*, found within this clay layer, is a freshwater species and occurs in low energy environment common in lakes (Maher et al, 1975).

Predating the deposition of the Amnicola Clay, southern California went through a tectonic transformation that made it possible for freshwater pluvial lakes to form in low-lying areas of the southern San Joaquin Basin. Atwater (1998) discusses the Plio-Pleistocene transpressional regime that occurred around 5 Ma when the Pacific plate captured Baja California. The new configuration resulted in a new inland plate boundary with two transpressional bends (Atwater, 1998). According to Bartow (1991), thrusting resulted from a compressional bend in the San Andreas Fault along the southern margin of the San Joaquin Basin generating a fold and thrust belt along the southern and western basin margins. This thrusting caused around 6 km of shortening in the San Joaquin Basin as well as 53 km of convergence in the Transverse Ranges in the past 2-3 Ma (Namson and Davis, 1988; Miller, 1999). The thrust belt partitioned the western part of the San Joaquin Basin into a series of northwest-trending anticlines and synclines. Uplift of the Coast Range along these thrusts began

around 6 Ma causing subsidence in the adjacent foreland by thrust loading and flexure of the underlying crust to form a foreland basin (Rentshler and Block, 1988).

During the Pliocene and continuing into the Pleistocene, the southern Sierra Nevada experienced accelerated uplift and west tilt that contributed to subsidence in the San Joaquin Basin (Rentschler and Bloch, 1988; Clark et al., 2005; Maheo et al., 2009). Cecil et al. (2014) concluded that rapid Pliocene subsidence rates of between 0.2-0.5 mm/yr are attributed to viscous coupling of dense delaminating eclogite root with the lower crust of the southwestern Sierra Nevada. The time of greatest subsidence occurred between 2.5 and 0.6 Ma which falls within the time that the Amnicola and the Tulare Clay were deposited (Cecil et al, 2014).

Deposition of the Amnicola Clay, and the older Blue seismic flooding event, likely occurred in the structurally low portions of the San Joaquin basin during a time of wetter than normal conditions. According to Clark et al. (2005), accelerated erosion from rapid river incision started less than 3.5 Ma in the Kern River and is related to climate change as well as the removal of the dense root beneath the Sierra Nevada which caused uplift (Peizhen et al., 2001). From 3.5 to 2.5 Ma higher amounts of precipitation were interpreted from soil carbonate isotopes, which lead to lacustrine highstands in Searles Lake and Tulelake (Forester, 1991; Smith et al., 1993). This time period would roughly correlate to the deposition of the Amnicola Clay in the Elk Hills area.

Starting around 1.25 Ma, low frequency (100 kyr) climate cycles began what is called the middle Pleistocene transition (Clark et al., 2006). During the period from about 1.25 Ma to 700 ka there was an increase in glaciation that resulted in the deposition of the Corcoran Clay when Lake Clyde filled the basin (Harden, 1999). Lake Clyde was a pluvial lake that resulted when the northern jet stream was pushed south from a large glacial episode causing increased precipitation

towards the end of the middle Pleistocene transition when maximum glaciations began (Negrini, 2002; Clark et al.,2006).

References

Anderson, F.M., 1905, A stratigraphic study in the Mount Diablo Range of California: California Acad. Sci. Proc., v. 3, no. 1, p. 1-40

Arnold, R. and Johnson, H.R., 1910, Preliminary report on the McKittrick-Sunset oil region, Kern and San Luis Obispo Counties, California: U.S. Geological Survey Bulletin 406, p. 1-225.

Atwater, T., 1970, Implications of plate tectonics of the Cenozoic tectonic evolution of the western North America: Geological Society of American Bulletin, v.81, p.3513-3536.

Atwater, T., 1998, Plate tectonic history of southern California with emphasis on the Western Transverse Ranges and Santa Rosa Island *in* Weigand, P.W., ed., Contributions to the geology of the Northern Channel Islands, southern California: AAPG Pacific Section, MP 45, p. 1-8.

Baron, D., Negrini, R.M., Golob, E.M., Miller, D., Sarna-Wojicki, A., Fleck, R.J., Hacker, B., and Erendi, A., 2008, Geochemical correlation and $^{40}Ar/^{39}Ar$ dating of the Kern River ash bed and related tephra ayers: Implications for the stratigraphy of petroleum-bearing formations in the San Joaquin Valley, California: Quaternary International, v. 178, p. 246-260.

Bartow, A. J., 1991, The Cenozoic evolution of the San Joaquin Valley, California: U.S. Geological Survey Professional Paper 1501, 40 p.

Berryman, W.M., 1973, Lithologic characteristics of Pliocene rocks cored at Elk Hills, Kern County, California: US Geological Survey Bulletin 1332-D, p. 1-53.

California Division of Oil, Gas, and Geothermal Resources (DOGGR), http://www.conservation.ca.gov/dog/Pages/Index.aspx, Accessed January 1, 2015.

Cecil, M.R., Saleeby, Z., Saleeby, J. and Farley, K.A, 2014, Pliocene-Quaternary subsidence and exhumation of the southeastern San Joaquin Basin, California, in response to mantle lithosphere removal: Geosphere, v. 10, no. 1, p. 129-147.

Clark, M.K., Maheo, G., Saleeby, J. and Farley, K.A., 2005, The non-equilibrium landscape of the southern Sierra Nevada, California: GSA Today, v. 15, no. 9, p. 4-10.

Clark, P.U., Archer, D., Pollard, D., Blum, J.D., Rial, J.A., Brovkin, V., Mix, A.C., Pisias, N.G. and Roy, M., 2006, The middle Pleistocene transition: characteristics, mechanisms, and implications for long-term changes in atmospheric pCO_2: Quaternary Science Reviews, v. 25, p.3150-3184.

Cobos, L. S., 2006, Seismic sequence stratigraphy of late Miocene to Pliocene sediments in the Elk Hills area, southern San Joaquin Basin: Unpub. M.S. thesis California State University Bakersfield, 139 p.

Crosby, T. W. and Schymichzek, H., 1990, An overview of oil field waste disposal as they relate to ground-water quality in the southern San Joaquin Valley, California *in* Kuespert, J.G. and Reid, S.A., eds., Structure, Stratigraphy and Hydrocarbon Occurrences of the San Joaquin Basin, California: AAPG Pacific Section, no. 65, p. 47-53.

Decelles, P.G., 1998, Middle Cenozoic depositional, tectonic, and sea level history of southern San Joaquin Basin, California: AAPG Bulletin, v. 72, no. 11, p. 1297-1322.

Dickinson, W.R., and Seely, D.R., 1979, Structure and stratigraphy of forearc region: AAPG Bulletin, v. 63, p. 2-31.

Fiore, P. E., Pollard, D. D., Currin, W. R., and Miner, D. M., 2007, Mechanical and stratigraphic constraints on the evolution of faulting at Elk Hills, California: AAPG Bulletin, v. 91, no. 3, p. 321-341.

Forester, R.M., 1991, Pliocene-climate history of the western United States derived from lacustrine ostracodes: Quaternary Science Reviews, v. 10, p.133-146.

Fresh water Gastropods Upper Pliocene Tulare Formation Kettleman Hills, King Country, California, http://inyo.coffeecup.com/site/kh/tularefm4.html, Accessed 10/19/2015.

Gester, G. G., 1917, Geology of a portion of the McKittrick district [Kern County], a typical example of west side, San Joaquin Valley oil fields, and a correlation of the oil sands of the west side fields: Proceedings of the California Academy of Sciences, v. 4, no. 7, p. 207-227.

Graham, S.A., Stanley, R.G. and Carter, J.B., 1989, Oligocene and Miocene paleogeography of central California and displacement along the San Andreas fault: Geological Society of America Bulletin, v. 101, p. 711-730.

Harden, D., 2003, Calofornia Geology, Prentice Hall, 552 p.

Harding, T. P., 1976, Tectonic significance and hydrocarbon trapping consequences of sequential folding synchronous with San Andreas faulting, San Joaquin Valley, California: The American Association of Petroleum Bulletin, v. 60, no. 3, p. 356-378.

Hilchie, D.W., 1979, Old electric log interpretation: Douglas W. Hilchie Inc., Boulder, Colorado, p.1-163.

Kiser, S.C., Greenwood, E.J., and Bazeley, L.M., 1988, Lithofacies of the Pleistocene to recent sediments in western Kern County, California; San Joaquin Geological Society, v. 7, p. 1-9.

Lillis, P. G., and Magoon, L. G., 2008, Petroleum systems of the San Joaquin Basin Province, California-geochemical characteristics of oil types: U.S. Geological Survey Professional Paper 1713, v. 1713-9, p. 1-52. http://pubs.usgs.gov/pp/pp1713/09/pp1713_ch09.pdf, accessed November 05, 2015.

Maheo, G., Saleeby, J., Saleeby, Z., and Farley, K.A., 2009, Tectonic control on southern Sierra Nevada topography, California: Tectonics, v. 28, p. 1-22.

Maher, J.C., Carter, R.D., and Lantz, R.J., 1975, Petroleum geology of Naval Petroleum Reserve No. 1, Elk Hills, Kern County, California: Geological Survey Professional Paper 912, 112 p.

McPherson, J. G., and Miller, D., 1990, Depositional settings and reservoir characteristics of the plio-pleistocene Tulare formation, south Belridge field, San Joaquin Valley, California *in* Kuespert, J.G. and Reid, S.A., eds., Structure, Stratigraphy and Hydrocarbon Occurrences of the San Joaquin Basin, California: AAPG Pacific Section, no. 65, p. 205-214.

Miller, D., 1999, Sequence stratigraphy and controls on deposition of the upper Cenozoic Tulare Formation, San Joaquin Valley, California: Unpub. PhD thesis, Stanford Department of Geological and Environmental Sciences, 198 p.

Namson, J. and Davis, T., 1988, Structural transsect of the western Transverse Ranges, California: implications for lithospheric kinematics and seismic risk elvaluation: Geology, v. 16, p. 675-679.

Negrini, R.M., 2002, Pluvial lake sizes in the northwestern Great Basin throughout the Quarternary Period *in* Hershler, R., Madsen, D.B. and Currey, D.R., ed., Great Basin aquatic systems history: Smithsonian Institute Press, p. 11-52.

Negrini, R., Baron, D., Gillespie, J., Horton, R., Draucker, A., Durham, N., Huff, J., Philley, P., Register, C., Parker, J., Haslebacher, T., 2009, A middle Pleistocene lacustrine delta in the Kern River depositional system: structural control, regional stratigraphy context, and impact on groundwater quality: Pacific Section AAPG Publication MP 48, p. 95-111.

Nicholson, G. E., 1990, Structural overview of Elk Hills *in* Kuespert, J.G. and Reid, S.A, eds., Structure, Stratigraphy and Hydrocarbon Occurrences of the San Joaquin Basin California, AAPG Pacific Section, no. 65, p. 133-140.

Page, R.W., 1983, Geology of the Tulare Formation and other continental deposits, Kettleman City area, San Joaquin Valley, California, with a section on ground water management

considerations and use of texture maps: U.S. Geological Survey, Water-Resources Investigations Report 83-4000, p. 1-24.

Peizhen, Z., Molnar, P., and Downs, W., 2001, Increased sedimentation rates and grain sizes 2-4 Myr ago due to the influence of climate change on erosion rates: Nature, v. 410, p. 891-897.

Pemberton, J.R., 1929, Elk Hills, Kern County, California: SP 4: Structure of Typical American Oil Fields, v. 2, p. 44-61.

Reid, S.A.,1995, Miocene and Pliocene depositional systems of the southern San Joaquin Basin and formation of sandstone reservoirs in the Elk Hills area, California, *in* Fritsche, A.E., ed., 1995, Cenozoic paleogeography of the western United States-II: Pacific Section SEPM, book 75, p. 131-150.

Reid, S.A., and McIntyre, J.L., 2001, Monterey Formation porcelanite reservoirs of the Elk Hills field, Kern County, California: AAPG Bulletin, v.85, p. 169-189.

Reid, S.A., 1990, Trapping characteristics of upper Miocene turbidite deposits, Elk Hills Field, Kern County, California, *in* Kuespert, J.G. and Reid, S.A, eds., Structure, Stratigraphy and Hydrocarbon Occurrences of the San Joaquin Basin, California: AAPG Pacific Section, no. 65, p. 141-156.

Rentschler, M.S. and Bloch, R.B., 1988, Flexural subsidence modeling of the Tertiary San Joaquin Basin, California *in* Graham, S.A., ed., Studies of the geology of the San Joaquin Basin: Pacific Section S.E.P.M., v. 60, p. 29-52.

Sarna-Wojcicki, A.M., 1976, Correlation of late Cenozoic tuffs in the Central Coast Ranges of California by means of trace- and minor element chemistry: Geological Survey Professional Paper 972, 30 p.

Smith, G.A., Wang, Y., Cerling, T.E. and Geissman, J.W., 1993, Comparison of a paleosol-carbonate isotope record to other records of Pliocene-early Pleistocene climate in the western United States: Geology, v. 21, p. 691-694.

Woodring, W.P., Roundy, P.V., and Fransworth, H.R., 1932, Geology and oil resources of the Elk Hills California: Geological Survey, Bulletin 835, p. 1-82.

Zumberge, J. E., Russell, J. A., and Reid, S. A., 2005, Charging of Elk Hills reservoirs as determined by oil geochemistry: AAPG Bulletin, v. 89, no. 10, p. 1347-1371.

Appendix 1- Amnicola Clay Formation Marker Depths and Thickness

Well Number	API Number	Top Amnicola Clay (MD)	Base Amnicola Clay (MD)	Amnicola Clay Thickness (ft)
326-25R	04029271090001	436.48	460.2	23.72
362-25R	04029271160001	283.58	316.94	33.36
348-28R	04029271750001	429.04	457.75	28.71
26-29R	04029271820001	511.78	546.66	34.88
551R-15Z	04029410330301	1070.92	1121.67	50.74
5-311-30R	04029518910001	619.44	649.75	30.31
9-387-25R	04029536860002	546.83	581.23	34.4
374-7R	04029681690002	892.13	970.21	78.09
385-X	04029765380100	1294.4	1339.93	45.54
322H-35R	04030005270001	620.49	651.92	31.43
313-30R	04030038630001	632.62	665.41	32.78
481-27R	04030292190000	555.13	587.5	32.37
45WD-27R	04030293400000	434.69	467.4	32.71
47WD-27R	04030293410000	476.71	509.82	33.1
48WD-27R	04030293420000	504.26	535.78	31.52
56WD-27R	04030293430000	460.85	489.4	28.54
58WD-27R	04030293690000	519.15	546.72	27.56
66WD-27R	04030293700000	525.08	553.74	28.67
77WD-27R	04030293710000	541.13	570.87	29.73
78WD-27R	04030293720000	558.35	587.52	29.16
82SW-9G	04030304210000	268.77	297.81	29.04
85S-2G	04030307200000	248.95	271.6	22.65
451-36R	04030308620000	439.27	462.42	23.15
447-25R	04030315430000	431.63	458.21	26.32
472-36R	04030316960000	536.51	580.45	43.7
12SW-1G	04030317920000	278.65	304.01	25.36
454-35R	04030318470000	602.07	627.16	24.9
433SW-33S	04030318480000	349.46	386.63	37.12
56WD-18G	04030318830000	1591.66	1644.15	52.45
33S-1G	04030329370000	216.24	247.86	31.62

32SE-1G	04030329380000	181.74	207.92	26.19
365-25S	04030332860000	583.55	595.39	11.84
31SE-4G	04030350960000	398.78	424.39	25.61
15WD-27R	04030336970000	475.24	506.36	31.12
17WD-27R	04030336980000	563.56	588.79	25.23
35WD-27R	04030336990000	509.14	543.64	34.5
36WD-27R	04030337000000	512.89	546.46	33.58
34WD-27R	04030338310000	489.7	523.01	33.3
86-34S	04030361720000	294.12	317.73	23.62
16A-35S	04030361730000	319.95	341.16	21.21
67SE-34S	04030361880000	300.99	325.25	24.25
21A-35S	04030348720000	95.16	124.19	29.03
332-36S	04030345020000	199.02	218.29	19.27
64WD-23Z	04030366580000	1133.97	1174.66	40.69
87WD-23Z	04030366630000	1002.99	1053.28	50.29
14SE-1G	04030366880000	302.91	320.74	17.84
81NW-34S	04030370920000	172.57	192.01	19.44
61X-34S	04030370940000	210.3	230.8	20.5
54E-29S	04030365030000	394.3	429.44	35.14
75N-29S	04030365040000	305.29	347.46	42.17
48NE-1G	04030365350000	357.43	377.23	19.8
32S-1G	04030365360000	333.36	356.05	22.68
48E-2G	04030365380000	246.35	276.73	30.38
63S-36S	04030365410000	372.95	401.11	28.16
86SW-29S	04030365980000	296.55	338.12	41.57
455-27R	04030365990000	476.32	510.49	34.18
482-28R	04030366000000	457.75	486.46	28.71
25NE-29S	04030363390000	209.43	236.02	26.59
24N-29S	04030363400000	280.93	311.25	30.28
36E-29S	04030363410000	208.13	235.69	27.56
16SW-28S	04030363430000	364.34	403.88	39.53

461-34R	04030356070000	566.7	594.06	27.35
66NE-9G	04030356350000	298.28	339.66	41.37
14XWD-27R	04030356530000	450	482.54	32.54
84XWD-28R	04030356540000	551.05	582.15	31.1
44S-4G	04030369050000	452.94	466.67	13.72
35NW-4G	04030369100000	405	431.75	26.75
17E-5G	04030369430000	415.95	436.11	20.16
48SE-5G	04030369470000	336.17	363.67	27.5
41SW-8G	04030369520000	422.55	459.39	36.83
48SW-36S	04030373610000	291.48	308.33	16.85
384X-31R	04030381170000	800.4	825.97	25.57
16NW-28S	04030388110000	395.57	435.98	40.41
44NW-1G	04030378480000	215.77	248.38	32.61
321-31S	04029274910001	380.7	410.07	29.37
82N-17G	04030393170000	869.93	917.17	47.12
66WD-23Z	04030399140000	1211.05	1258.06	47.01
622-24R	04030400430000	622.27	658.56	36.29
12WD-27R	04030412300000	424.77	458.02	33.37
54WD-23Z	04030412340000	1154.64	1206.02	51.35
55WD-23Z	04030412350000	1206.93	1248.49	41.08
56WD-23Z	04030412360000	1201.72	1248.1	46.21
52WD-28R	04030414070000	570	601	30.81
62WD-28R	04030414080000	558.8	588.87	30.12
82WD-28R	04030414090000	518.97	548.23	29.47
62X-1G	04030415630000	511.82	527.59	15.76
56W-1B	04030410000000	541.83	575.16	33.33
14SE-12G	04030410020000	542.79	574.25	31.46
44E-34R	04030431010000	483.42	499.86	16.44
45E-34R	04030431020000	497.75	515.13	17.38
66E-34R	04030431060000	480.06	499.09	19.02
87E-34R	04030431110000	530.31	551.23	20.92

58WD-21R	04030427980000	588.79	618.99	30.2
68WD-21R	04030427990000	582.57	613.72	31.15
88WD-21R	04030428000000	485.33	514.77	29.44
18WD-22R	04030428010000	404.58	434.51	29.93
42SW-2G	04030428320000	369.21	392.64	23.42
72N-17G	04030428370000	769.69	816.19	46.5
53WD-23Z	04030423540000	1079.26	1134.31	55.09
21WD-27R	04030418350000	386.52	417.45	31.01
51WD-28R	04030418360000	581.96	613.25	32
61WD-28R	04030418370000	524.72	550.27	25.56
81WD-28R	04030418380000	397.94	427.44	29.95
84-29S	04030433600000	416.17	454.46	38.26
37-27R	04030438140000	460.71	493.4	32.68
33NE-17G	04030438200000	1090.75	1153.71	62.87
24WD-27R	04030438550000	380.19	418.88	38.69
16WD-22R	04030451380000	425.46	457.01	31.54
26WD-22R	04030451390000	412.67	449.76	37.09
27WD-22R	04030451400000	395.57	430.15	34.58
28-30R	04030451930000	678.5	720.72	42.22
35-30R	04030451940000	636.87	667.2	30.33
22WD-28R	04030452870000	492.84	523.94	31.1
31WD-28R	04030452880000	549	587	38
32WD-28R	04030452890000	479.4	508.79	29.38
42WD-28R	04030452900000	560.66	595.37	34.71
37-20R	04030453090000	449.76	477.71	27.95
41WD-28R	04030453270000	582.37	621.38	39.01
11WD-28R	04030453550000	455.36	484.06	28.71
12WD-28R	04030453560000	418.72	447.35	28.63
21WD-28R	04030453570000	517.75	554.34	36.59
11-27R	04030437200000	428.13	456.11	27.98
23-27R	04030437330000	387.76	416.54	28.78

24-27R	04030437340000	432.71	463.16	30.4
34-27R	04030437350000	453.27	486.79	33.53
57WD-21R	04030447560000	615.12	645.34	30.22
87WD-21R	04030447580000	513.93	546.95	33.02
56WD-21R	04030442280000	603.49	631.85	28.36
21-19R	04030468910000	585.73	616.7	30.97
37	04029014690000	1182.76	1227.5	44.74
542-7B	04029036860100	1299.69	1359.91	60.22
367	04029094110100	991.5	1033	41.5
18	04029094130000	1187.47	1241.89	50
1	04029253880000	855.25	912.95	60
381-26Z	04029270260000	858.78	905.75	46.96
378	04029270890000	360.54	390.85	30.31
88-24R	04029271030000	354.48	386.79	32.32
358-26R	04029271390000	540.24	565.94	25.69
352-27	04029271590000	530.64	565.98	35.33
24-28R	04029271630000	472.1	508.79	36.68
366-29	04029271970000	463.25	502.54	39.29
62-33R	04029272190000	451.67	489.95	38.28
65-33R	04029272210000	431.65	467.29	35.64
24-34R	04029272340000	433.67	466.84	33.18
312-34R	04029272440000	498.07	534.98	36.91
382R	04029272470000	584.38	619.26	34.88
86-35R	04029272530000	573.42	601	27.58
41-30S	04029274560000	287.13	318.14	31.01
322-31	04029274920000	450.65	480.57	29.91
348	04029274980000	413.93	447.38	33.45
352-31	04029274990000	267.18	300.25	33.07
322H-32S	04029275440100	354.8	385.23	30.43
116	04029276570000	227.53	261.76	34.24
346-34S	04029276630100	382.27	431.67	36.69

280	04029277690000	128.36	150.69	22.33
3-88	04029277850000	297.98	319.54	21.56
25	04029290380000	370.49	395.85	25.37
36	04029290450000	367.16	391.67	24.51
45	04029290500000	352.2	378.05	25.85
322H-5G	04029291090100	381.31	412.11	30.8
13-6G	04029291160000	433.04	475	41.96
24-6G	04029291190000	370.67	413.73	43.06
64-6G	04029291330000	461.4	506.75	45.35
73-6G	04029291370000	401	431	30
85	04029375430000	828.2	879.34	51.15
16	04029375580000	1235.37	1289.22	53.85
27	04029375610000	1195.34	1246.72	51.37
1	04029375720000	686.95	723.2	36.25
344-7R	04029480090000	889.77	952.47	62.7
342-7R	04029480100000	1007.85	1086.72	78.87
355-7R	04029480670000	857.86	921	63.14
322-17R	04029488710000	651.95	719.47	67.52
346-8R	04029492870000	828.91	885.75	56.85
78-6G	04029505320000	411.74	453.64	41.9
55-5G	04029516330000	389.7	416.46	26.76
24-5G	04029516380000	407.81	443.36	35.55
28-4G	04029517030000	338.67	358.44	19.77
313-4G	04029522780000	382.44	415.67	33.23
27-6G	04029527950000	448.72	496.69	47.97
11-33S	04029528000000	339.73	370.25	30.53
16-28S	04029528340000	385.82	424.47	38.66
38-8G	04029528710000	712.98	775.34	62.35
74	04029534590000	450	479.5	29.5
335-16R	04029544650000	640.8	694.7	53.91
333-4G	04029545290000	341.5	373.62	32.12

382-5G	04029545300000	339.08	367.32	28.24
322-2B	04029560620000	568.02	595.08	27.06
341-31S	04029561350000	342.06	374.21	32.15
71-33R	04029565050000	483.65	514.77	31.12
58-19S	04029565070000	412.86	446.67	33.81
356-34R	04029573330000	462.16	483.95	21.79
544-14Z	04029585110100	763.28	882.48	60
332A-36R	04029586740000	560.5	600.87	40.37
81-17G	04029596030000	761.95	823.79	61.84
375-26R	04029602850000	550.62	579.28	28.66
357-7R	04029621500000	808.2	896.37	88.18
338-24R	04029623800000	436.32	473.14	36.82
358-24R	04029626890000	396.91	427.98	31.06
345-24Z	04029628870000	615.19	652.51	37.32
345-7R	04029647890000	826.9	893.43	66.53
328A-31S	04029665900000	475.55	507.93	32.37
346-29R	04029668650000	501.33	527.24	25.9
366A-24Z	04029668660000	573.44	605.58	32.15
71-30S	04029669720000	522.25	562.95	40.7
345-28R	04029670980000	532.71	566.2	33.49
23X-17G	04029672660000	1133.99	1181.63	47.64
73-33R	04029674270000	450.19	481.75	31.56
377-23R	04029680910000	365.25	392.18	26.93
41-36R	04029682220000	467.62	495.97	28.35
331X-36R	04029685800000	493.02	536.4	43.38
342-32S	04029686820000	521.57	555.47	33.9
328-13Z	04029688790000	749.68	783.47	33.79
83-34R	04029724710000	503.39	535.11	31.72
934-29R	04029746510000	486.52	512.99	26.47
356XH-26R	04029785790100	565.94	596.57	30.63
376-24Z	04029809770000	557.09	595.65	38.56

365H-35R	04029899260000	570.95	602.7	31.74
338X-36R	04029899600000	525.19	565.67	40.48
382H-27R	04030005260000	535.46	570.56	35.09
328-27R	04030007970000	540.85	568.94	28.1
318-30R	04030015800000	663.04	693.36	30.32
316X-30R	04030018820000	705.26	741.53	36.27
312H-26R	04030020010000	471.74	511.84	40.04
368-23R	04030023030000	442.09	468.66	26.57
372X-36R	04030023700000	419.37	452.07	32.69
313H-26R	04030026990000	488.32	528.63	40.31
321H-36R	04030027540000	563.54	598.98	35.44
341-17R	04030028010000	733.08	787.74	54.65
366H-26R	04030028920000	582.32	613.82	31.5
318-24R	04030033250000	408.3	441.26	32.95
388H-26R	04030034380000	581.21	615.03	33.83
318-34S	04030034450000	352.49	389.8	37.31
361-17R	04030035230000	753.33	819.45	66.12
332H-36R	04030045090000	565.91	605.12	39.22
377H-26R	04030046190000	583.94	619.86	35.91
26NE-2G	04030112310000	355.02	384.39	29.37
27-2G	04030118700000	364.71	388.5	23.79
37X-14B	04030118820000	1395.42	1439.87	44.44
38S-36S	04030119060000	175.31	205.95	30.63
42E-10G	04030119780000	206.83	241.66	34.84
13X-35S	04030123330000	144.39	171.68	27.29
153H-36R	04030125000000	483.69	510.62	26.93
72NE-2G	04030136750000	297.5	334.3	36.79
76S-24Z	04030143310000	550.62	576.76	26.15
87W-4G	04030154040000	301.45	339.79	38.34
47A-2G	04030161500000	255.16	286.68	31.52
76N-9G	04030165660100	326.09	367.2	41.11

78-35R	04030167570000	565.04	594.32	29.27
83NE-9G	04030176920000	240.61	276.03	35.43
54SE-2G	04030178650000	255.01	286.7	31.7
26SW-29S	04030188080000	209	236.54	27.53
27WD-18G	04030210080000	1533.82	1587.62	53.8
44NE-10G	04030213750000	180.74	219.51	38.77
66NE-36S	04030220600000	122.34	141.88	19.54
18E-36S	04030220800000	417.38	436.12	18.74
25NW-1G	04030224870000	296.23	320.56	24.33
33SW-1G	04030224890000	254.36	285.49	31.13
52XSE-1G	04030231030000	256.51	278.99	22.47
35SW-36S	04030251660000	255.48	288.49	33.01
38NW-36S	04030252530000	189.28	221.89	32.59
38E-36S	04030253400000	198.09	227.73	29.63
345XH-28R	04030257690000	539.09	570.19	31.1
13NW-1G	04030258250000	215.08	247.24	32.16
23W-1G	04030258280000	191.51	222.64	31.12
13S-35S	04030259500000	142.38	174.76	32.38
358X-25R	04030260660000	405.93	434.85	28.91
84NE-35S	04030260840000	208.39	241.66	33.26
85NE-35S	04030260850000	180	213.76	33.75
16W-36S	04030260880000	211.91	233.93	22.01
417X-26R	04030276070000	536.5	567.84	31.33
45NW-36S	04030276100000	282.69	308.84	26.16
415X-27R	04030279540000	525.7	559.35	33.64
86S-2G	04030280390000	246.91	273.49	26.59
25SW-4G	04030281520000	297.84	323.83	25.96
28N-36S	04030281550000	164.43	199.02	34.59
18X-36S	04030281570000	310.08	331.82	21.74
62X-17G	04030456240000	919.55	971.21	51.66
76-1G	04030456360000	457.27	478.03	20.76

38WD-21R	04030456620000	587.95	618.54	30.59
45WD-21R	04030456630000	616.92	644.98	28.06
46WD-21R	04030456640000	626.74	668.84	42.09
47WD-21R	04030456650000	604.76	643.11	38.35
48WD-21R	04030456660000	598.04	625.8	27.76
55WD-21R	04030456670000	588.61	621.62	33.01
75WD-21R	04030456690000	425.62	459.92	33.86
17WD-21R	04030456730000	567.23	606.28	39.05
18WD-21R	04030456740000	563.56	596.29	32.73
26WD-21R	04030456760000	614.65	653.71	39.04
15WD-22R	04030457320000	384.28	419.68	35.22
72S-9G	04030461600000	450.5	473.47	22.97
54E-24Z	04030464550000	658.05	688.72	30.66
65XN-24Z	04030464590000	629.23	655.83	26.6
22X-31R	04030470860000	688.01	718.35	30.34
31-31R	04030470870000	688.01	718.34	30.32
11SE-19R	04030477160000	668	703	34.95
81-24Z	04030477730000	655.31	681.47	26.12
56-19R	04030484220000	636.28	667.79	31.42
63E-9G	04030489160000	417.48	438.83	21.36
82W-17G	04030489180100	902.81	951.52	48.69
31E-7G	04030489210000	449.26	488.68	39.41
11S-3G	04030497930000	448.55	485.16	36.6
44	04029017660000	738.16	805.84	67.69
51	04029017670000	1282.46	1336.15	53.69
72	04029017740000	1227.25	1287.59	60.34
513	04029018240000	917.29	965.45	48.16
524	04029018650000	654.75	679.67	24.92
552	04029018790000	694.53	751.33	56.81
44-19G	04029022760000	1529.81	1602.75	72.94
82-19G	04029022880000	1578.32	1665.29	86.97

90-19G	04029022920000	1584.66	1661.87	77.22
216-19G	04029022970000	1349.8	1428.45	78
1-1	04029022990000	1546.09	1621.9	75.81
2-4-19G	04029023380000	1520.71	1601.39	80.68
2-5-19G	04029023390000	1413.99	1489.36	75.37
90-29G	04029023700000	1617.32	1705.41	88
202-29G	04029023730000	1567.34	1650.29	82.95
54	04029099160000	663.65	715.65	52
63	04029174060000	1403.03	1468.11	65.09
69	04029174070000	1534.11	1606.29	72.19
16-35R	04029272490000	505	535.83	30.83
22-35R	04029272500000	597.83	621.95	24.12
24-35R	04029272510000	540.48	566.81	26.34
28-36R	04029272600000	501.88	534.36	32.49
314-36	04029272660000	502.6	530.93	28.34
312A	04029272790000	568.32	588	19.68
316-31	04029274900000	491.49	524.55	33.06
378	04029275040000	500.04	526.8	26.76
474	04029275340000	211.5	241.53	30.03
31-34S	04029276410000	276.55	312.85	36.31
51-34S	04029276510000	221.74	245.43	23.69
344	04029277780000	270.79	303.95	33.16
62-1B	04029278820000	552.03	600.35	48.31
62	04029278910000	562.42	597.1	34.68
46	04029278960000	1313.28	1397.21	83.93
67-1G	04029279180000	300.58	318.23	17.64
87	04029279200000	288.24	313.11	24.88
85	04029290160000	335.78	358.5	22.72
15-9G	04029291640000	351.28	398.24	46.96
25	04029291910000	200.7	245.53	44.83
36	04029291950000	228.72	271.36	42.64

52-10G	04029291980000	155.74	194.84	39.1
63-10G	04029291990000	147.69	181.27	33.58
81-10G	04029292030000	235.71	259.77	24.06
86-10G	04029292040000	295.81	331.01	35.2
1NO21-15	04029292250000	636.27	671.08	34.8
42-16G	04029292260000	891.14	947.98	56.83
15-14B	04029292540000	1499.36	1541.7	42.33
26-14B	04029292570000	1448.94	1484.34	35.4
27-14B	04029292580000	1297.69	1337.64	39.94
36-14B	04029292600000	1498.7	1557.05	58.35
47	04029292630000	1480.95	1530.6	49.65
57-14B	04029292640000	1498.87	1544.65	45.78
58-14B	04029292650000	1377.13	1427.93	50.79
53-22	04029380560000	2427.76	2494.42	65.38
1-2-19G	04029414790000	1506.56	1570.95	64.4
79	04029504040000	914.47	965.79	51.32
16-5G	04029505220000	393.36	413.53	20.18
73-1B	04029510440000	489.54	530.83	41.29
47-6G	04029510520000	379.5	424.38	44.88
67-6G	04029510560000	434.82	477.72	42.91
85-6G	04029510580000	389.25	409.19	19.94
87-5G	04029516310000	273.82	303.41	29.59
58-5G	04029516320000	340.35	373.02	32.67
47-5G	04029516340000	369.45	401.73	32.29
35-5G	04029516350000	396.89	420	23.11
27-4G	04029517020000	364.85	393.32	28.47
43-4G	04029517050000	340.36	374.78	34.42
65-8G	04029518210000	366.29	428.64	62.35
32-8G	04029518260000	370.98	427.7	56.72
351-4G	04029522760000	354.04	383.33	29.29
16-10G	04029522900000	325.85	367.73	41.89

52-36R	04029526760000	492.81	519.99	27.18
85-1B	04029527400000	480.13	518.24	38.11
58-8G	04029528570000	697.54	739.3	41.76
38-9G	04029529460000	520.23	562.96	42.74
317-34S	04029529830000	324.32	357.51	33.18
41-1B	04029529870000	510.02	554.11	44.09
35-36R	04029530510000	559.02	598.05	39.03
331	04029532330000	389.5	420.4	30.9
331-3G	04029532960000	359.31	392.65	33.33
14-4G	04029533910000	346.74	374.93	28.18
371-4G	04029536330000	441.13	475.64	34.51
313-5G	04029536800000	383	417.66	34.66
377-33S	04029537310000	348.88	386.3	37.42
61H	04029538790000	511.6	547.65	36.05
47-8G	04029539220000	651.9	706.05	54.14
83-4G	04029541380000	431.79	462.33	30.55
78X-9G	04029541450000	433.41	466.18	32.76
311-4G	04029543100000	435.44	460.68	25.24
28-6G	04029547320000	490.33	533.83	43.5
353-3G	04029556100000	374.88	405.64	30.76
67X-8G	04029556200000	516.02	558.66	42.64
12-12G	04029556290000	476.95	501.3	24.35
42-2B	04029556740000	565.89	594.79	28.9
12-8G	04029559750000	320.6	363.11	42.51
62X-8G	04029559760000	344.09	367.24	23.15
54-1B	04029561500000	512.98	560.75	47.77
88-33S	04029564390000	504.53	541.22	36.69
351-2B	04029566580000	569.36	598.64	29.29
313-2G	04029579420000	372.46	395.41	22.95
48X-9G	04029584210000	408.03	470.14	62.11
286-1B	04029584990000	475.17	518.69	43.52

326-35R	04029586730000	526.97	555.87	28.9
41-17G	04029596040000	828.24	871.59	43.35
318-32S	04029628030000	402.51	431.15	28.64
81WD-1	04029644490000	810.46	879.74	69.28
314-5G	04029653810000	394.98	426.7	31.72
88WD-7G	04029654950000	620.13	675.32	55.19
33-17G	04029657740000	1196.48	1252.55	56.08
78WD-7G	04029666890000	718.29	786.82	68.53
15-1B	04029668500000	629.48	662.62	33.14
71-2B	04029668520000	552.4	584.77	32.37
77-35R	04029669430000	602.46	624.15	21.69
13-17G	04029675550000	1266.23	1315.18	48.95
31-16G	04029713100000	697.79	751.67	53.88
26-1B	04029720520000	629.7	670.64	40.94
16-3G	04029773130000	370.15	407.86	37.71
352X-3G	04029845290000	411.25	447.75	36.5
311-5G	04029851550000	414.8	445.72	30.92
352-6G	04029879850000	476.62	509.68	33.06
221-15G	04030003350000	640.39	677.04	36.65
328X-32S	04030007430000	379.54	409.33	29.79
85A-10G	04030012900000	278.32	309.95	31.63
66WD-12B	04030032390000	815.06	870.93	55.87
86WD-12B	04030032400000	742.99	805.71	62.72
22WD-12B	04030033240000	700	738	38
45-9G	04030038210000	329.34	390.24	60.9
67-11G	04030039660000	474.14	525.49	51.36
46WD-7G	04030040290000	960.33	1018.64	58.31
77A-10G	04030045120000	297.19	330.46	33.28
28-35R	04030112290000	538.2	567.72	29.52
48S-4G	04030165700000	294.93	328.03	33.11
68SW-34S	04030177920000	274	297	23

44-31T	04030184840000	952.26	977.54	19.05
52SE-33S	04030186910000	313.31	349.41	36.1
41N-10G	04030187220000	215.23	242.56	27.33
48-31T	04030189460000	871.77	889.27	17.05
457-31S	04030192340000	462.54	492.06	29.52
72N-4G	04030192350000	443.12	479.54	36.42
52NW-17G	04030200670000	873.95	913.07	39.12
37WD-18G	04030210090000	1573.45	1621.29	47.12
57WD-13B	04030221310000	1219.88	1262.51	42.63
27SW-31T	04030223800000	877.66	891.17	13.52
87SE-3G	04030225040000	264.39	289.6	25.2
21SW-10G	04030228320000	251.06	285.14	34.09
38A-WD-8G	04030246320000	721.13	775.93	54.79
47WD-13B	04030250500000	929.58	979.83	50.25
45SE-34S	04030257700000	552.28	577.58	25.3
335-31S	04030262320000	505.01	534.13	29.12
374X-1G	04030269830000	230.21	253.86	23.65
14WD-13B	04030272110000	1005.26	1079.86	74.59
636H-25B	04030440140000	858.71	881.09	22.38
5-6	04029012630000	861.67	924.34	62.67
588	04029012880000	983.31	1028.09	44.78
62X	04029013400000	1361.13	1418.74	57.6
13-25Z	04029014750000	739.9	792.02	52.12
61	04029014790000	1281.83	1331.3	49.47
12	04029016770000	1413.36	1470.49	57.13
13	04029016780000	1569.2	1614.19	44.99
21	04029016820000	1478.86	1527.21	48.35
32	04029016860000	1461.03	1506.59	45.56
41	04029016900000	1530.16	1579.77	49.61
45	04029016940000	1397.01	1455.35	58.34
63	04029017010000	1538.27	1577.95	39.68

74	04029017070000	1512.38	1557.13	44.75
77	04029017100000	1201.89	1245.81	43.92
233	04029017160000	1463.05	1503.12	40.07
17	04029017780000	610.38	649.92	39.54
41	04029017830000	579.47	630.89	51.42
561-21B	04029017930000	646.73	696.62	49.9
561-29B	04029020220000	625.28	655.85	30.57
71A	04029020250000	618.5	655.56	37.05
13-5M	04029032760000	1422.03	1441.93	19.89
1-5-35Z	04029036810000	682.47	748.4	40.52
45	04029052650000	850.9	907.4	56.5
567-16Z	04029052780000	1032.9	1104.23	71.34
10-10	04029053580000	487.94	527.17	39.23
343-15Z	04029094190000	1018.27	1059.38	41.11
354-15Z	04029094220000	1018.66	1068.41	49.75
363-15Z	04029094250000	999.3	1043.05	43.75
515	04029094360000	920	970	50
548-15Z	04029094440000	1077.91	1119.77	41.87
564	04029094480000	931.96	989.33	57.36
4-7	04029094590000	1019.99	1071.72	51.73
47K	04029094960000	528.61	560.75	32.14
1	04029154450000	1101.32	1158.28	56.95
3	04029178930000	683.64	754.58	24.88
2	04029251020000	974.99	1026.54	45
67-28S	04029274170000	270.49	300.66	30.16
42	04029358840000	1010.94	1059.52	48.58
A-1	04029358910000	490.92	510.78	45.11
5	04029360370000	763.32	798.05	34.73
24	04029374530000	1300.72	1346.85	46.13
46	04029374550000	1340.96	1389.62	48.15
551	04029410330100	342.09	362.97	20.88

523	04029411950000	1416.58	1459.28	42.69
377-30	04029413660000	615.18	646.2	31.02
545	04029415040000	673.93	710.02	36.08
564	04029433040000	1176.23	1226.49	48.31
535-25Z	04029434410000	820.03	867.32	47.29
521-26S	04029452960000	221.27	240.08	18.81
535	04029463860000	1330.45	1379.25	48.8
1-8	04029467800000	930.95	997.07	66.12
311-17R	04029486950000	631.1	690.84	59.73
2-2W	04029488410000	1069.81	1117.82	48.02
1-2CW	04029488440000	1057	1108	51
16-20R	04029491010000	363.75	390.94	27.18
46-30R	04029491980000	647.04	675.89	28.85
10-2	04029499370000	823.01	867.05	44.04
352-24Z	04029505470000	657.08	694.58	37.5
322-24Z	04029510370000	698.3	723.54	25.24
333-24Z	04029510380000	667.23	704.25	37.02
313-24Z	04029513490000	729.8	763.48	33.68
386-24Z	04029513510000	590.8	620.69	29.89
332-24Z	04029514110000	720.1	752.94	32.84
317-26R	04029516980000	544.64	577.75	33.12
77	04029517300000	619.43	650.38	30.95
383-27R	04029523260000	546.45	580.01	33.56
315-15R	04029528380000	562.02	603.43	41.41
68-25R	04029532480000	469.15	496.69	27.55
68-25R	04029532490000	459.71	499.23	39.53
337-15R	04029534930000	706.68	742.33	35.64
315-25R	04029535040000	482	509	27
A17	04029536840000	685.04	787.46	46.53
73-30S	04029548490000	449.94	483.23	33.29
324X	04029554280000	1453.07	1514.47	61.4

10	04029554550000	507.05	551.76	44.72
63-26R	04029555650000	516.96	547.75	30.8
56-28R	04029555670000	508.2	536.07	27.86
14-1A	04029557150000	881.94	914.08	32.14
65-29R	04029557510000	461.22	500.24	39.02
347-25R	04029565030000	373.91	402.64	28.73
85-29S	04029566850000	386.3	426.96	40.66
355-14R	04029568180000	721.09	760.12	39.03
357-15R	04029573890000	578.25	615.17	36.92
317-13R	04029575040000	733.8	771	37.2
537-14R	04029575740000	559.39	598.49	39.1
47-19S	04029578850000	460.02	489.36	29.34
57W-20S	04029589530000	356.28	394.62	38.34
328-25R	04029590430000	480.95	508.89	27.94
328-23R	04029590440000	480.17	514.01	33.84
64-24R	04029591760000	470.17	503.4	33.23
358-13Z	04029592370000	700.49	737.49	37.01
348-23R	04029592380000	477.89	508.64	30.75
386A-26R	04029592390000	533.29	564.78	31.48
364-26R	04029592480000	551.61	579.77	28.16
36X-34R	04029594170000	544.79	563.9	19.12
346-19R	04029594470000	557.56	586.83	29.27
383-29R	04029611240000	448.04	476.14	28.1
354-23R	04029617570000	402.94	435.27	32.33
35	04029632300000	668.85	689.18	20.33
346-32R	04029633930000	952.15	984.98	32.83
382-25Z	04029650850000	621.18	658.62	37.44
377-8B	04029655840000	1309.48	1358.88	49.4
386-30R	04029666970000	609.2	634.81	25.62
566-20R	04029668550000	500.14	532.35	32.21
341-29R	04029669560000	393.71	431	37.29

316-32R	04029673470000	921.77	946.1	24.33
55-34R	04029680160000	428.51	449.88	21.37
43-33R	04029680170000	404	439.9	35.9
322A-26R	04029682890000	474.99	514	39.01
331-26R	04029685590000	547.31	583.94	36.64
333X-26R	04029685930000	575.18	615	39.82
327-23R	04029686410000	460.49	493.94	33.45
316A-24R	04029686420000	523.09	553.05	29.96
354X-17R	04029686430000	677.32	737.46	60.13
386-17R	04029688080000	695.08	737.62	42.54
311-26R	04029689370000	528.01	566.31	38.3
337X-23R	04029692240000	452.62	479.77	27.15
377-19R	04029692710000	464.67	495.14	30.47
384-30R	04029692720000	591.33	618.17	26.84
325X	04029696510000	822.43	856.28	33.85
383X	04029699820000	690.26	731.9	41.64
346X-36Z	04029708570000	695.43	732.03	36.59
371X-25R	04029716430000	329.31	363.02	33.71
1A	04029717830000	930.67	964.2	33.53
27NE-30R	04029720650000	682.95	717.08	34.13
2-1AW	04029723620000	1130.91	1174.61	43.7
366-25Z	04029724630000	631.03	674.06	43.02
384X-7R	04029729320000	969.77	1047.85	78.09
364X	04029739750000	792.05	819.29	27.24
100	04029748310000	719.51	769.27	49.76
86X-5	04029818820000	1504.14	1524.84	20.05
337A-24Z	04029831000000	694	730	36
CH1-27R	04029861360000	579.08	614.2	35.12
375X-23R	04029879830000	416.31	445.68	29.36
44-29R	04030108090000	406.49	434.53	28.05
47-29R	04030108100000	466.52	497.93	31.41

77SE-BM-26	04030127920000	186.04	216.23	30.19
88-25S	04030176980000	598.52	616.28	17.76
88NE-29S	04030186900000	333.83	368.97	35.14
76BM-26S	04030193400000	588.87	603.27	14.4
25-25S	04030234370000	573.85	587.66	13.82
442A-34R	04030259750000	512.16	545.46	33.29
416-34R	04030265280000	614.69	636.1	21.4
455-34R	04030265290000	421.32	453.86	32.54
474-27R	04030279530000	573.63	604.26	30.63
54WD-27R	04030279850000	484.7	514.15	29.45
44WD-27R	04030279860000	458.48	485.74	27.26
463-33R	04030287620000	431.97	471.42	39.45
371-23	04029270380000	915.78	944.23	28.45
311	04029270400000	1077.27	1102.43	25.16
48	04029270610000	540.46	570.72	30.26
314-18	04029270620000	734.11	799.5	65.39
366-19	04029270650000	512.12	545.68	33.56
538-19	04029270670000	557.21	585.08	27.87
328-20	04029270700000	332.67	364.85	32.18
86-22R	04029270750000	448.51	485.51	37
378-22	04029270770000	534.21	564.98	30.77
62-23R	04029270800000	334.92	363.57	28.65
82-23R	04029270820000	451.93	483.33	31.4
322-23	04029270850000	456.93	493.57	36.64
338-23	04029270860000	565.56	602.56	36.99
356-23	04029270870000	396.73	430.58	33.84
372-27	04029271600000	538.5	569.25	30.75
4-84	04029271850000	513.52	546.09	32.57
321-29	04029271890000	298.86	325.29	26.43
324-29	04029271900000	418.74	454.56	35.82
343-29R	04029271930000	407.83	437.85	30.02

515-29R	04029272020000	564.25	595.87	31.62
362	04029272080000	614.71	641.82	27.11
61-32R	04029272130000	494.33	522.11	27.78
42-33R	04029272170000	406.92	435.39	28.46
242-33	04029272230000	405.92	434.66	28.74
358	04029272250000	712.26	732.32	20.06
58-34R	04029272390000	539.36	569.62	30.26
64-34R	04029272410000	447.25	484.55	37.3
477	04029272420000	505.04	522.74	17.7
23	04029375370000	1112.06	1162.27	50.2
76	04029375520000	1205.42	1262.56	57.14
2	04029375670000	677.31	707.33	30.02
1	04029371510000	1140.86	1194.37	53.51
542	04029372040000	666.06	696.14	30.07
342	04029278940000	544.92	570.96	26.03
16N-14B	04030521650000	1418.73	1459.4	40.67
46-35R	04030518780000	586.79	611.31	24.52
17SW-4G	04030533760000	465.39	495.67	30.29
537-4Z	04029036760000	1389.56	1436.16	46.6
64X-32	04029114070000	2396.72	2447.7	50.99
88-4	04029212330000	1211.13	1258.92	47.79
1	04029365150000	1367.15	1384.42	46.02
1	04029366220000	1512.65	1547.98	35.33
1	04029394140000	997.1	1041.97	45
11X	04029574670000	1279.65	1321.81	42.17
374X-6R	04030244080000	1559.22	1627.19	67.96
68NE-14B	04030542070000	1472.15	1542.89	70.74

Appendix 2-Tulare Clay Formation Tops and Thickness

Well Number	API Number	Top Tualre Clay (MD)	Base Tulare Clay (MD	Tulare Clay Thickness (ft)
54XWD-18G	04030317910000	357.36	525.13	167.77
56WD-18G	04030318830000	631.99	726.53	94.53
72N-17G	04030428370000	518.54	549.26	30.72
33NE-17G	04030438200000	681.43	720.72	39.25
542-7B	04029036860100	546.47	594.84	48.37
2282WS-14B	04030186750000	304.39	561.19	256.8
27WD-18G	04030210080000	727.86	846.17	118.31
62X-17G	04030456240000	664.17	699.14	34.96
51	04029017670000	473.65	493.13	19.49
44-19G	04029022760000	410.19	444.59	34.39
82-19G	04029022880000	456.55	511.39	54.84
1-1	04029022990000	422.71	453.52	30.81
2-4-19G	04029023380000	400.92	450.22	49.3
2-5-19G	04029023390000	303.79	362.95	59.16
60	04029024580000	1061.92	1165.52	103.6
223	04029024700000	1017.9	1122.96	105.06
4-8	04029024770000	1152.12	1252.81	100.69
69	04029174070000	417.84	451.12	33.28
1-B	04029238500000	476.59	940.05	463.46
15-14B	04029292540000	291.94	396.75	104.81
27-14B	04029292580000	305.62	348.12	42.51
57-14B	04029292640000	567.43	599.48	32.05
35	04029372820000	413.76	527.61	113.86
53-22	04029380560000	506.84	1167.5	471.63
71	04029389550000	610.98	1078.95	299
8-4-19G	04029413780000	668.72	827.78	159.05
1-2-19G	04029414790000	389.05	414.32	25.27
58-8G	04029528570000	464.85	492.79	27.93
86W	04029659800000	768.45	873.93	105.48
13-17G	04029675550000	469.88	595.54	125.66

138WD	04029858210000	568	627	59
58WD-7G	04029858220000	480.08	535.15	55.07
284WS-13B	04029869410000	509.04	613.9	104.86
45WS-18G	04029893870000	397.54	562.31	164.77
27WD	04030023010000	540.71	579.35	38.65
46WD-7G	04030040290000	596.5	656.93	60.44
52NW-17G	04030200670000	628.3	654.83	26.54
57WD-18G	04030202550000	721.6	859.74	138.14
67WD-18G	04030202560000	750	880.53	130.53
37WD-18G	04030210090000	318.48	834.08	136.97
77WD-13B	04030213780000	641.77	754.13	112.36
87WD-13B	04030213790000	691.93	806.28	114.35
45WD-13B	04030221300000	475.86	675.26	199.4
65WD-13B	04030221320000	502.19	711.17	208.98
85WD-13B	04030221330000	537.24	749.67	212.43
38A-WD-8G	04030246320000	494.5	534.12	39.61
17WD-13B	04030250470000	333.18	482.18	149
25WD-13B	04030250480000	406.9	599.88	192.98
35WD-13B	04030250490000	373.24	644.89	199.08
47WD-13B	04030250500000	340.07	477.48	137.42
44WD-13B	04030272140000	457	652.56	195.56
54WD-13B	04030272150000	498.37	615.21	116.84
25-18G	04030415420000	590.78	721.64	130.86
62X	04029013400000	661.93	703.02	41.08
13	04029016780000	415.06	483.52	68.46
21	04029016820000	414.38	507.19	92.81
32	04029016860000	410.66	475.23	64.57
41	04029016900000	437.25	537.91	100.65
63	04029017010000	446.42	520.53	74.11
74	04029017070000	437.87	494.4	56.53
77	04029017100000	615.78	669.83	54.05

1	04029154450000	202.48	247.91	45.44
9A	04029197900000	929.61	1058.02	128.41
10	04029197910000	963.07	1071.05	107.98
11	04029197920000	947.69	1045.46	97.77
5	04029360370000	292.84	329.43	38.54
377-8B	04029655840000	418.91	513.57	94.66
1	04029371510000	511.29	547.49	36.21
68NE-14B	04030542070000	552.71	590.48	37.77

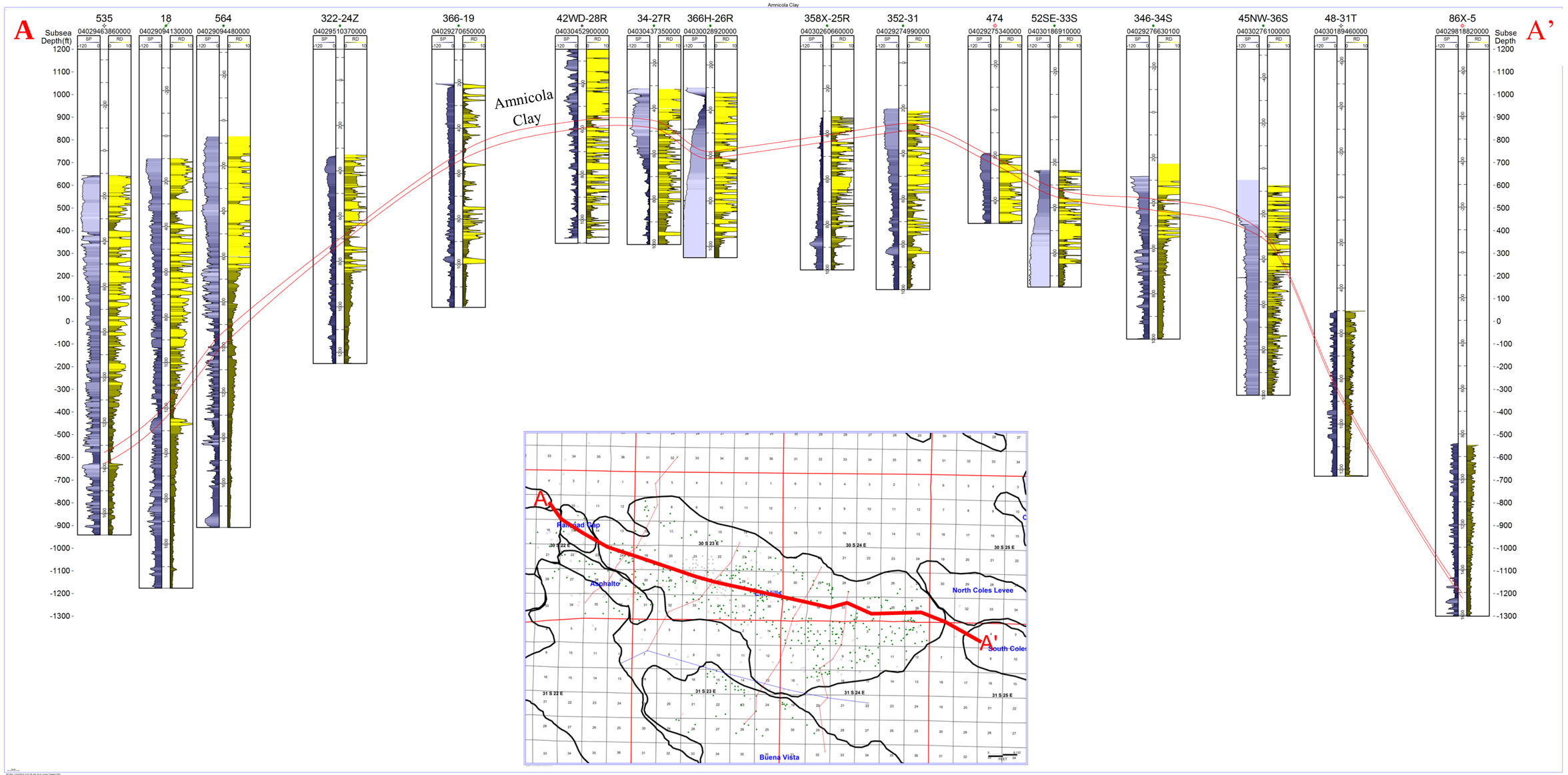

Appendix 3. West to east cross section A-A’ showing structure on top of the Amnicola Clay (Outlined in red).

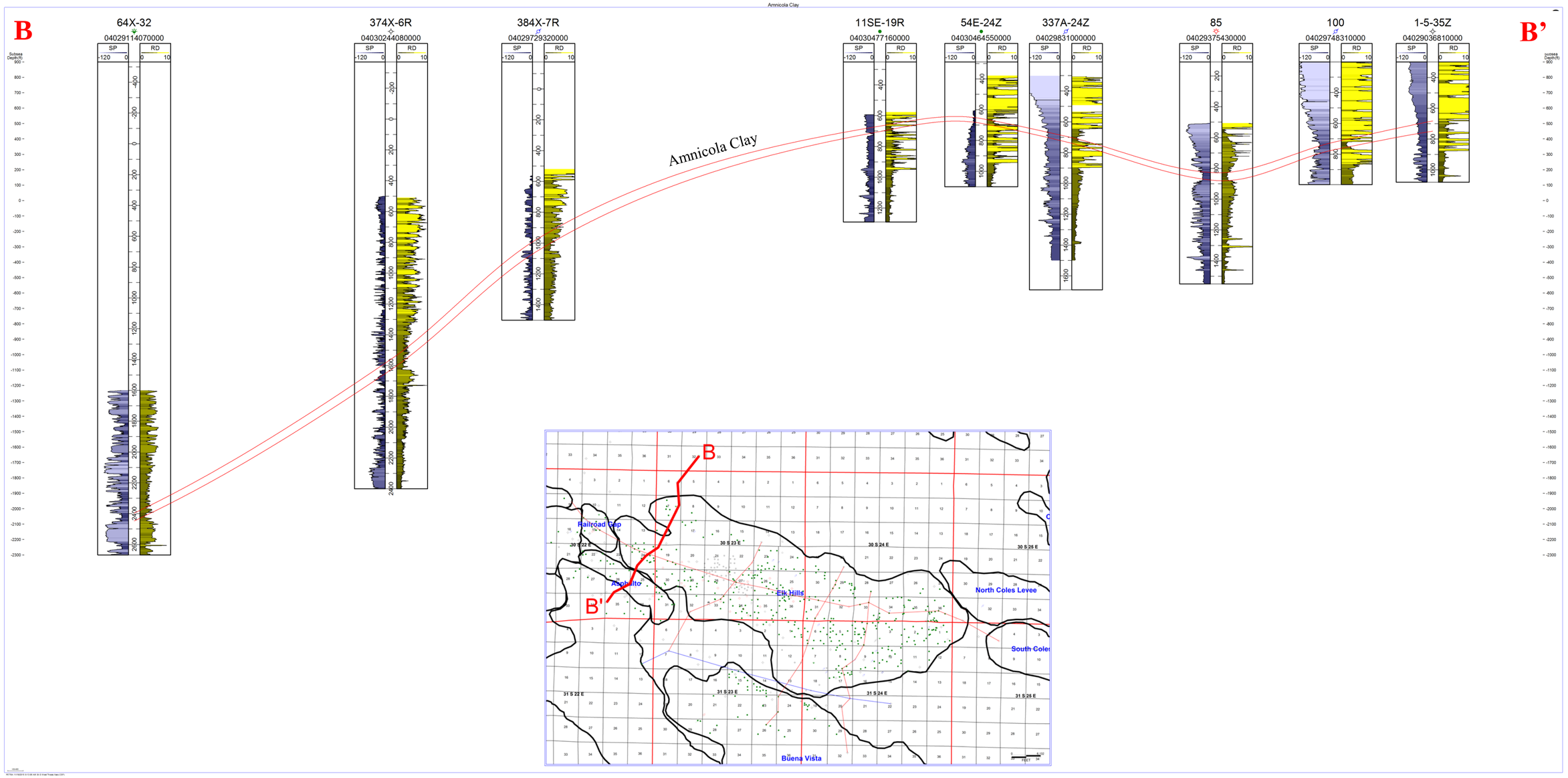

Appendix 4. Northeast to southwest cross section B-B’ showing structure on top of the Amnicola Clay (Outlined in red).

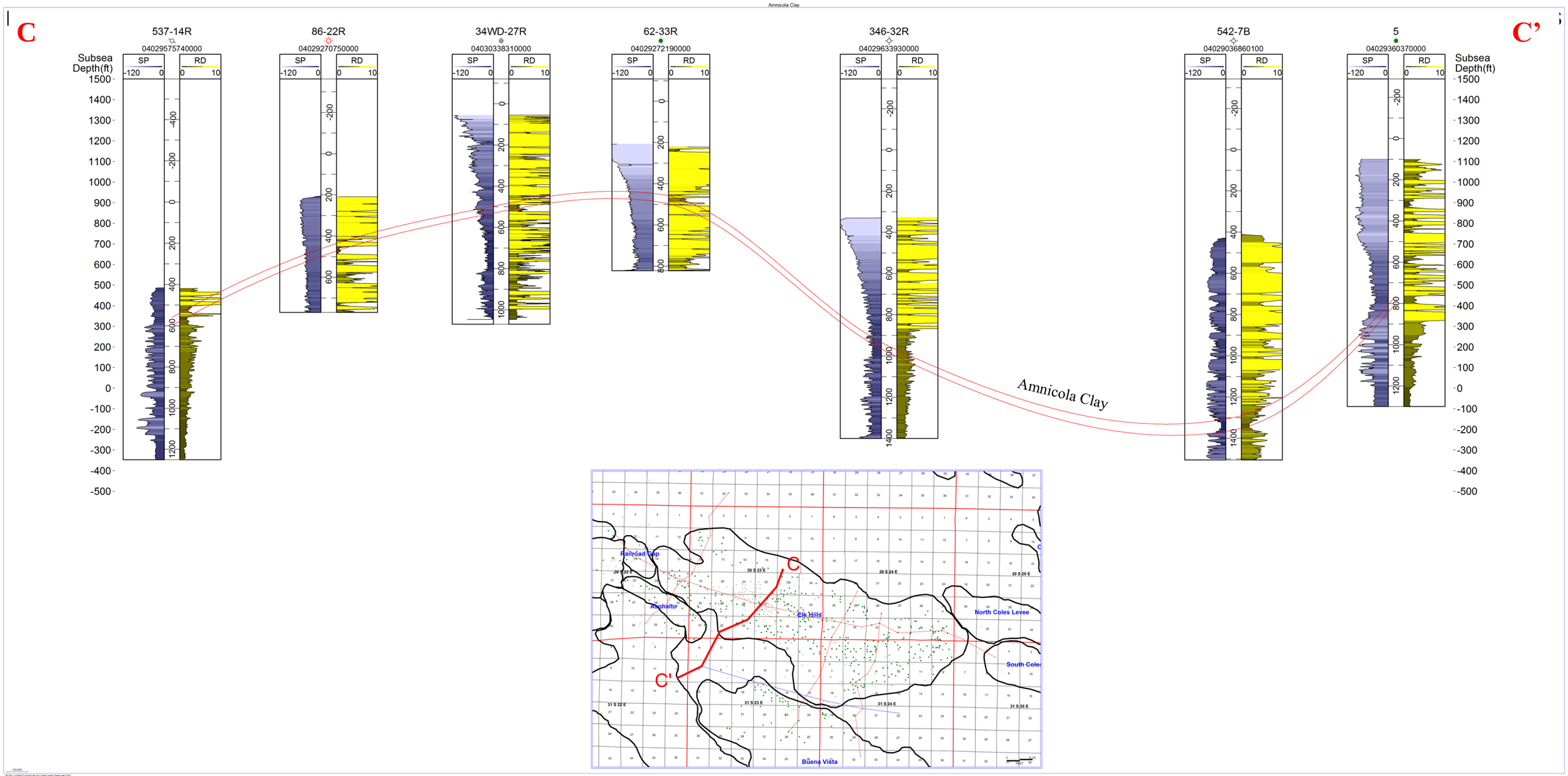

Appendix 5. Northeast to southwest cross section C-C’ showing structure on top of the Amnicola Clay (Outlined in red).

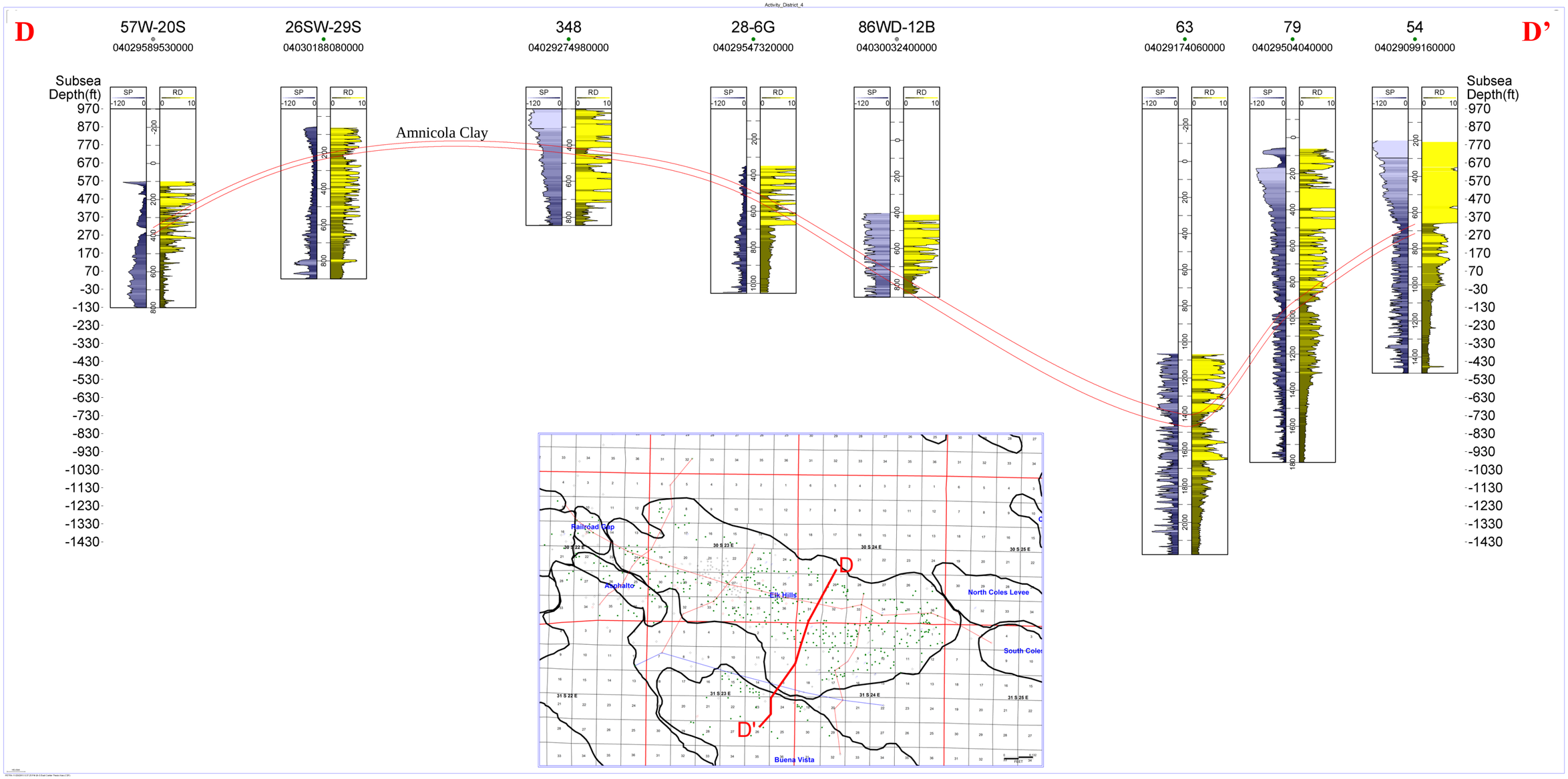

Appendix 6. Northeast to southwest cross section D-D’ showing structure on top of the Amnicola Clay (Outlined in red).

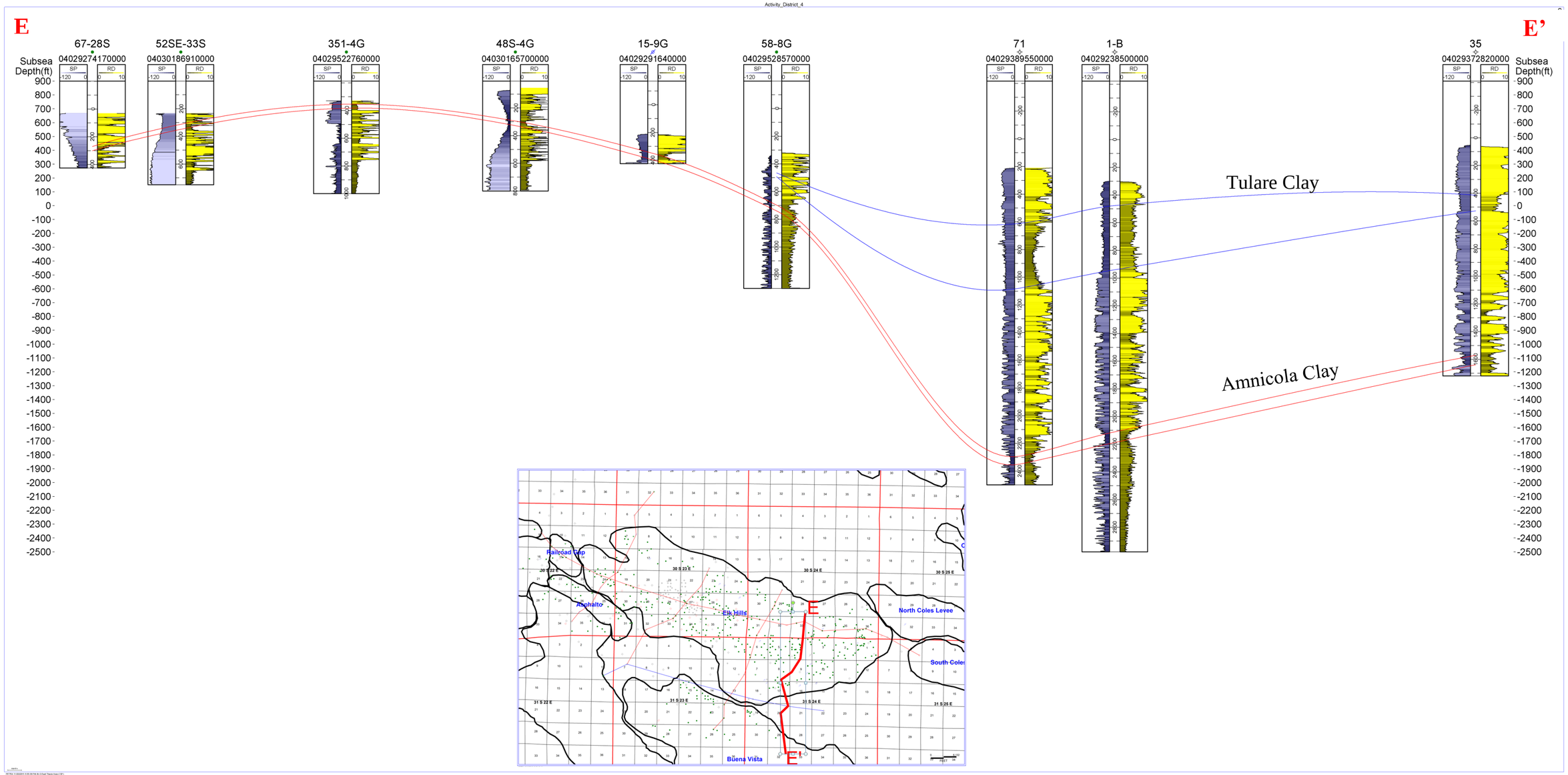

Appendix 7. North to south cross section E-E’ showing structure on top of the Amnicola Clay (Outlined in red) and Tulare Clay (outlined in blue).

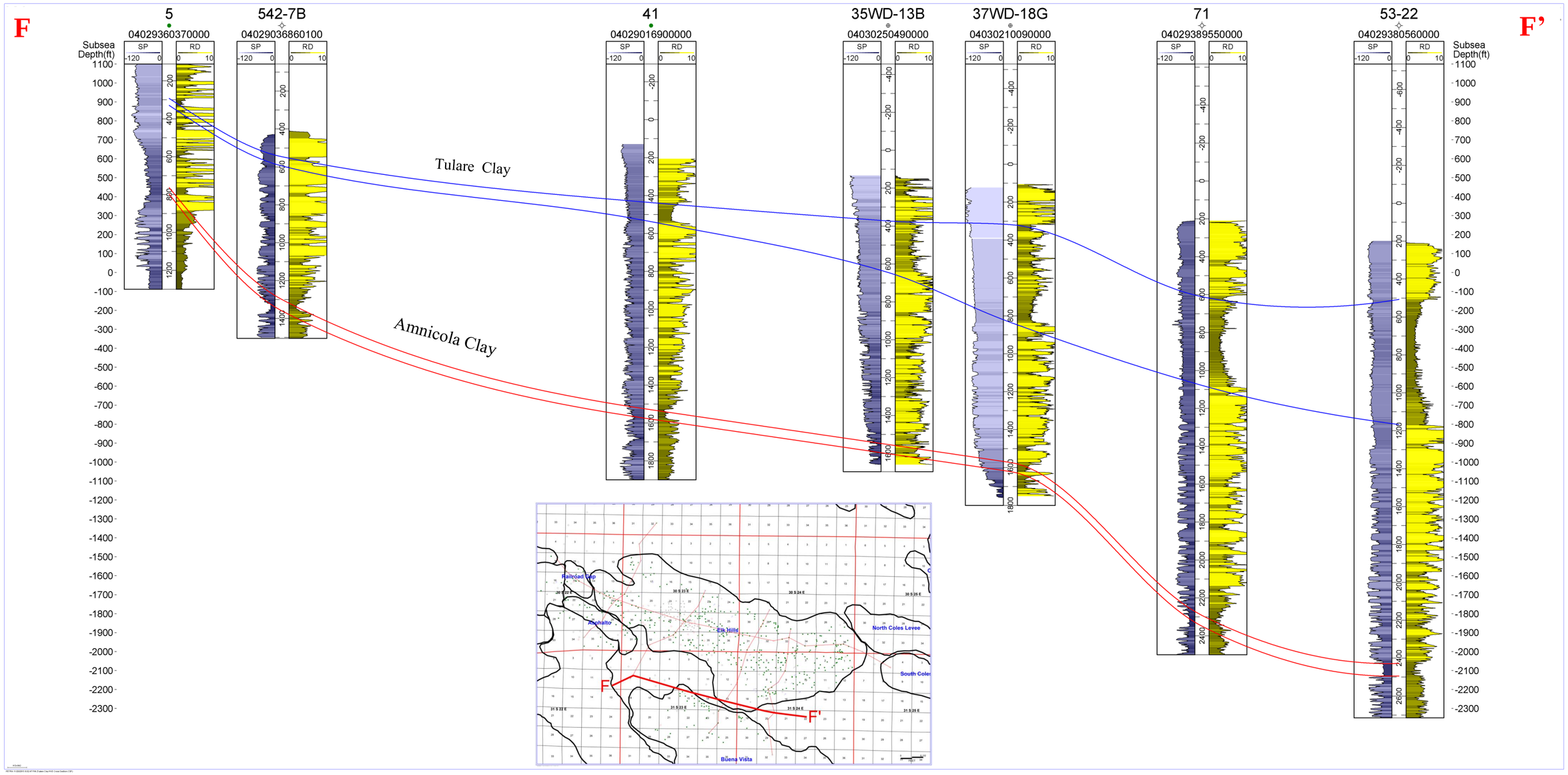

Appendix 8. West to east cross section F-F’ showing structure on top of the Tulare Clay(outlined in blue) and the Amnicola Clay (outlined in red).